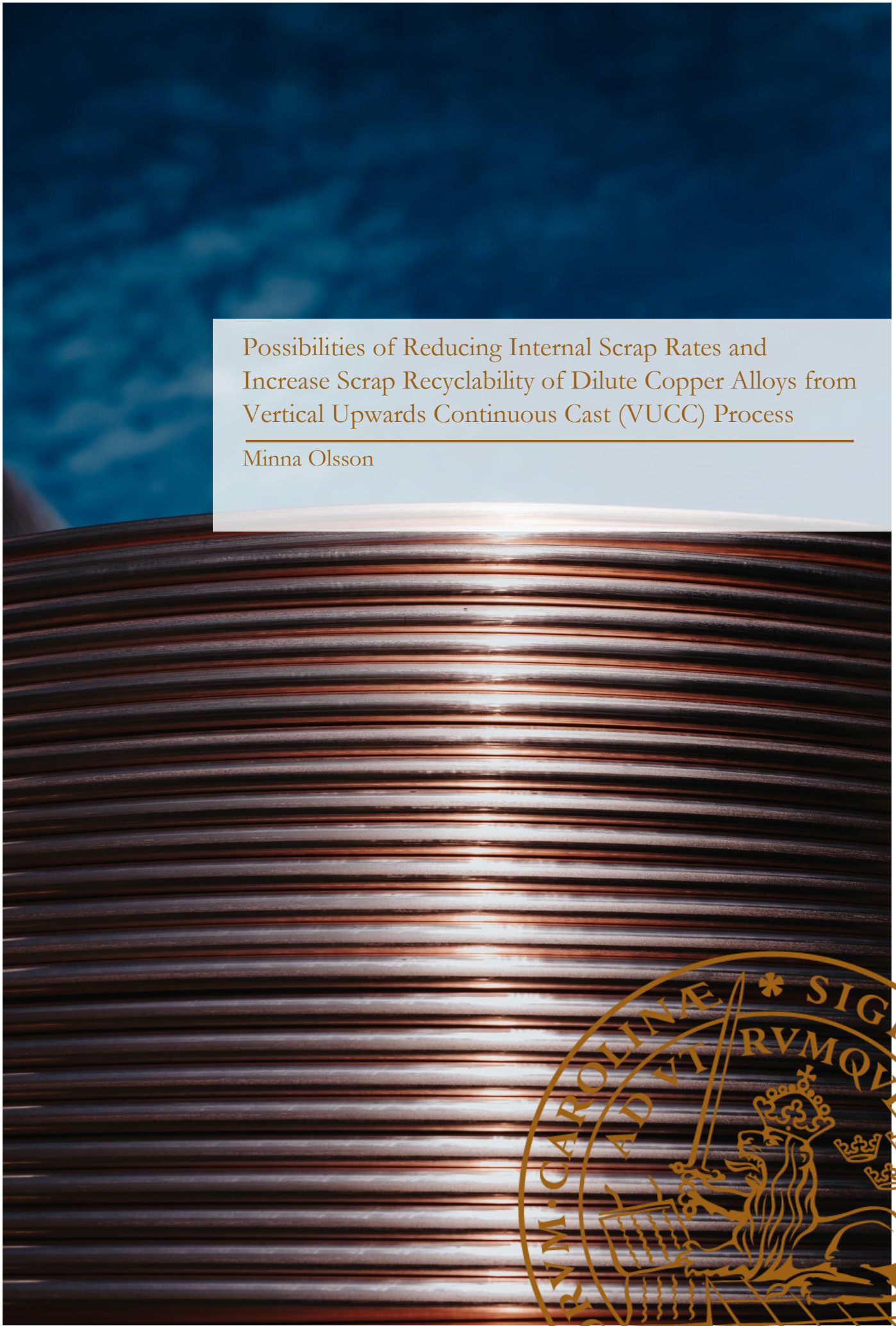

Possibilities of Reducing Internal Scrap Rates and Increase Scrap Recyclability of Dilute Copper Alloys from Vertical Upwards Continuous Cast (VUCC) Process

Minna Olsson

Possibilities of Reducing Internal Scrap Rates and Increase Scrap Recyclability of Dilute Copper Alloys from Vertical Upwards Continuous Cast (VUCC) Process

By

Minna Olsson

Centre for Analysis and Synthesis
Lund University
&
Elcowire AB

February 2023

Supervisor (LTH): Prof. Reine Wallenberg
Co-Supervisor (Elcowire AB): Marie Moses
Examiner: Prof. Jan-Olle Malm

Postal Address
P.O. Box 124
SE-221 00 Lund, Sweden
Web Address
www.lth.se/chemeng/

Visiting Address
Naturvetarevägen 14

Telephone
+46 46-222 82 85
+46 56-222 00 00
Telefax
+46 46 222 45 26

Abstract

Copper and copper alloys are important material systems for the electrification of society. The high workability of the materials makes them appropriate in numerous different applications which require highly conductive properties. One main advantage of Cu and Cu-bearing alloys is the eminent ability to be repeatedly recycled without losing the advantageous properties. This raises the question whether scrap alloys from secondary copper production can be reintroduced into continuous copper casting processes to increase the overall recyclability. The primary goal was to identify current scrap rates from the Vertical Upwards Continuous Cast (VUCC) process and assess methods to increase scrap recyclability. Scrap from the VUCC process was found to constitute of 16% of the total monthly production volume of CuMg0.49 alloy with a diameter of 30 mm at Elcowire AB. Scrap originated mainly from the process start-up phase and also from process related issues. Studies were carried out to evaluate if additional 400 ppm Mg decreased the start-up time and scrap rate. The method showed no beneficial results to decreasing the start-up time and further assessments are needed. No negative effect was observed regarding coil composition, but instead indicated the difficulties to control the Mg content in the melt throughout production. Mg losses to slag were found by the means of SEM and XEDS as MgO particles. The exposed Cu melt must therefore be more sufficiently protected, where an inert Ar gas flux may be applied. There is currently no feasible method to incorporate scrap into the VUCC process without redesigning the entire process. Produced scrap may instead be used in the SCR® rolling mill during ETP copper production, where results showed that the impurity content must be controlled, and Mg content is the main limiting factor. Further assessments are needed in terms of contaminant contribution to slag formation, effect on finished ETP copper and economic viability. The method does, however, show great promise and can be applied to various Cu-bearing alloys.

Acknowledgements

I would like to extend my gratitude to my two supervisors, Reine Wallenberg and Marie Moses, for all the help and encouraging words during this project. I would also like to thank my examiner, Jan-Olle Malm, who has always been a present figure throughout my years at LTH. This project would also not have been possible without the machine operators and my colleagues at Elcowire AB, from which I have learned a lot from.

I would also like to thank Daniel Madsen and Crispin Heatherington for all their time and support during the SEM analysis. Dmytro Orlov and his talented students also helped me immensely. I will never again underestimate the time required to polish a copper sample.

Special thanks to my family and friends, who have always supported me throughout my life and during my studies. Lastly, great thanks to my two opponents Hanna Sjöman and Amalia Emmoth for your valuable feedback. Without you and all the people I have met during my studies, my time at LTH would not have been the same.

Popular Scientific Summary

With the increasing need to diminish the usage of hydrocarbon-based fuels, metals are excellent to ease the transition into a more electrified society. Copper is one of the most important metals due to its natural abundance on our planet and its great properties. From its discovery several centuries ago, the usage of copper has continued to greatly increase. This is because the metal can be modified to suit several different applications by additions of other elements and by different manufacturing processes. It can be recycled over and over again, maintaining the important properties. This project focused on recycling of copper scrap from a casting process during production of copper wires used in products we can find all around us, for instance in trolley wire and wind turbines. To assess the recyclability, it was also important to determine the current scrap rates from the process itself.

Copper and copper alloys as wire products are typically produced in continuous casting processes. This makes it possible to produce wires of desired lengths. Properties such as strength and electrical conductivity are important. One available continuous casting process is the Vertical Upwards Continuous Cast (VUCC) process and is commonly used in production of oxygen-free copper alloys. Oxygen-free copper has a very low oxygen content, ensuring high wire purity and high electrical properties. The high electrical conductivity can be kept by keeping the alloying content low whilst also making the material stronger and more durable. Examples of alloying elements include additions of magnesium, silver, and tin.

During production of oxygen-free copper with low additions of magnesium from the VUCC process, 16% (approximately 30 tonnes) of scrap were produced over a month. The scrap comes from the process start-up phase, but also from process related issues. An attempt was made to minimise start-up scrap by adding extra magnesium before process weekend standstill. The extra addition would work as a buffer, as some magnesium is expected to be lost during production due to its low density compared to copper and low boiling temperature.

It was found that a portion of magnesium is lost to slag, which makes it difficult to keep the magnesium at strict levels in the copper melt and finished product. This is because magnesium readily reacts with oxygen. It is therefore important to protect the copper melt from oxidation. Although such measures are already applied for the VUCC process, improvements can always be made. One example would be to use argon gas to protect exposed copper melt, minimising the contact with oxygen in the surrounding atmosphere. Argon is inert, meaning it does not partake in chemical reactions.

Scrap coils were found difficult to directly recycle in the VUCC process. Instead, produced scrap can be introduced into another continuous casting process equipped with a rolling mill which produce thinner wires. Here it is important to assess other present elements in the scrap as impurities and how they affect the finished wire in terms of strength and conductivity. For example, too much magnesium can make the wire more brittle.

This project will act as a guide to further investigate what can be done to minimise produced scrap and scrap recyclability. The next step would be to try to melt different scrap and determine the wire composition by analytical techniques, then compare with the theoretical calculations presented in this report.

Populärvetenskaplig Sammanfattning

Med det ökande behovet att minska användandet av fossila bränslen så är metaller ett utmärkt alternativ för att elektrifiera samhället. Koppar är en av de viktigaste metallerna på grund av de stora mängder som förekommer naturligt på vår planet. Det är även på grund av dess utmärkta egenskaper. Sedan koppar upptäckes för flera århundraden sedan har användandet fortsatt att öka. Koppar och dess egenskaper kan ändras för att passa flertalet olika tillämpningar och produkter. Detta görs genom att tillsätta andra grundämnen eller genom att bearbeta metallen genom olika tillverkningsprocesser. Koppar kan även återvinnas om och om igen utan att förlora dess goda egenskaper. Detta projekt fokuserade på återvinning av koppar skrot från en gjutningsprocess som tillverkar koppartråd till produkter som är överallt runtomkring oss, exempelvis till kontaktledningar och vindkraftverk. För att utvärdera återvinningsmöjligheter är det också viktigt att fastställa nuvarande skrotmängder.

Koppar och kopparlegeringar som tråd tillverkas vanligen i stränggjutningsprocesser. Detta möjliggör att tillverka tråd av önskad längd. Egenskaper som hållfasthet och elektrisk konduktivitet är viktiga. Vertikala stränggjutningsprocesser används vanligtvis för att producera syrefritt koppar. Syrefritt koppar har ett väldigt lågt syreinnehåll, vilket bibehåller trådens renhet och höga konduktans. Den höga konduktiviteten kan bevaras genom att låglegera koppar, vilket samtidigt gör materialet starkare och mer hållfast. Exempel på legeringsämnen som kan tillsättas till koppar är magnesium, silver och tenn.

Vid vertikal stränggjutning av syrefritt koppar med låga tillsatser av magnesium så uppstod 16% (nästan 30 ton) skrot under en månad. Skrotet kommer främst från uppstartsfasen, men även på grund av processproblem. Ett försök gjordes att minska uppstartsskrot genom att tillsätta extra magnesium innan processens helgstillestånd. Den extra tillsatsen skulle fungera som en buffert, då en del magnesium förväntas försvinna och brännas av på grund av dess låga densitet och låga koktemperatur.

Det fastställdes att magnesium går förlorat till slagg i processen. Detta gör det svårt att bibehålla korrekta magnesiumnivåer i kopparsmältan och i den färdiga tråden. Detta är på grund av att magnesium lätt reagerar med syre. Därför är det viktigt att skydda kopparsmältan från oxidering. Förebyggande åtgärder tillämpas redan, men det finns alltid utrymme för förbättring. Ett exempel hade varit att använda argongas för att skydda blottad kopparsmälta genom att minska kontaktytan mellan smälta och omgivande syre i miljön. Argon är ett inert grundämne, vilket innebär att det mindre lätt deltar i kemiska reaktioner.

Skrotspolar är svåra att direkt återvinna i stränggjutningsprocessen. Istället kan uppstått skrot användas i en annan gjutningsprocess som är utrustad med ett valsverk för att producera tunnare tråd. Det är viktigt att utvärdera hur andra grundämnen som finns i skrotet som orenheter påverkar tråden och dess egenskaper. Som exempel så bidrar en förhöjd magnesiumhalt till att tråden blir mer skör.

Detta projekt kommer fungera som en guide för att fortsätta undersöka vilka metoder som kan användas för att minska producerat skrot och öka återvinningsgraden av skrot. Ett naturligt nästa steg vore att smälta ned blandat skrot och testa den slutliga kompositionen med hjälp av diverse analysmetoder. Sedan jämföra faktiska värden med de teoretiska beräkningarna som presenterats i denna rapport.

List of Abbreviations

BCC	Body-Centred Cubic
DP	Diamond Paste
ECCI	Electron Channeling Contrast Imaging
ETP	Electrolytic Tough-Pitch (Copper)
FCC	Face-Centred Cubic
IACS	International Annealed Copper Standard
ICSG	International Copper Study Group
OES	Optical Emission Spectroscopy
OF	Oxygen-Free (Copper)
SEM	Scanning Electron Microscopy
VUCC	Vertical Upwards Continuous Casting
XEDS	X-Ray Energy Dispersive Spectroscopy

Table of Contents

1 Introduction

The use of copper and copper products dates back several centuries. The malleable and readily engineered metal has shown to be of utmost importance for the electrification of society. This has led to an immense increase in copper ore mining and production of Cu materials and Cu-bearing alloys. Due to its advantageous properties, Cu is highly applicable in many areas in the form of rods, coils, and ingots. Its high electrical conductivity makes it suitable in both small electrical applications and high-voltage systems. Cu is commonly found in the renewable energy sector in solar panels and wind turbines, as well as in the automotive industry. Its durability is also prominent in the industrials sector for machinery and construction materials. The statistical database International Copper Study Group (ICSG) has reported that the global usage of Cu has increased with an annual growth rate of 3.4% since 1900 to 2020, emphasising the importance of copper in modern society [1].

This growth instinctively raises the question whether copper resources will eventually run out. But along with global growth, an increasing number of new ore reserves are identified. Technological advancements have made it possible to further the yield of primary Cu from ore, not to mention the introduction of recycled Cu. Occurring scrap from production routes is a valuable resource to obtain a higher material recyclability and decrease the use of new raw materials. Regarding environment and sustainability goals, the main advantage of Cu and Cu scrap is that it is readily recyclable as the metal does not lose its advantageous properties [1, 2].

Produced copper scrap can be classified as deriving from either internal or external sources and comes from several parts of industrial production and post-manufacture products. From primary copper producers, scrap occur during the manufacture of anodes and cathodes, which are vital feedstock materials for the downstream industry production of wires and rods. Secondary scrap emanates from these internal manufacturing processes, where alloying elements and coatings may have been added. In turn, these additions impose a greater challenge to assess appropriate recycling methods. Secondary production processes are continuously being developed to incorporate Cu scrap and scrap alloys to a larger extent [1, 2]. External sources include those from consumer and End-of-Life (EoL) products, such as automotive wires, electrical applications, and construction materials. It is that reported over 30% of the global demand of copper is today met with secondary Cu scrap and EoL products. Products are increasingly becoming more complex, demanding better and more efficient recycling routes. Considerations regarding scrap condition, location including transportation, alloying elements and impurities as well as government directives, are all important factors to determine the viability of scrap recycling [3, 4]. Since 2007, several global projects are ongoing to investigate industrial use of copper and manufacture scrap, as reported by ICSG and its membership countries. Published reports and surveys assess process capacity regarding usage, scrap rate and its growing demands. Economic and technological interests are evaluated, along with changes in regulatory requirements regarding recycling and trade [1].

Elcowire AB is one of Europe´s leading suppliers of Cu and Al wire and rod solutions. Their products are used globally in electrical systems to make infrastructural advances, such as in wind farms, electrical vehicles and to further develop railways. With a sustainable mindset, Elcowire AB continues to promote their projects to ease the transition from a hydrocarbon-based to an electrified society [5].

1.1 Project Goals

The main objective of the project is to assess which method is the most suitable in reducing internal scrap rates from the Vertical Upwards Continuous Casting (VUCC) process. For this it is necessary to evaluate the current scrap rates, the scrap types and origin, and chemical composition. The project will centre around emanating scrap during production of oxygen-free dilute CuMg0.49 alloy. It is therefore of interest to investigate the possibilities of maintaining a strict magnesium limit to ensure product quality and reduce occurring scrap. An evaluation regarding if and how the scrap can be incorporated into the manufacturing processes at Elcowire AB will be made. This includes the scrap recyclability into a rolling mill for ETP copper production and how the chemical composition of utilised the scrap will affect the final product. As a secondary objective, an attempt was also made to assess the microstructure of CuMg0.49 to gain further knowledge of compositional differences within the alloy.

1.2 Project Boundaries

This project will act as a guideline for Elcowire AB to further their work in scrap reduction and recyclability. An economical evaluation of the proposed methods is out of scope for this report. The project was limited due to the decision to shut down the VUCC process. This hindered the investigation period, including data collection, possible analyses and especially implementation of the proposed methods. It was not feasible to incorporate scrap from the VUCC into the rolling mill and analyse the effect of present elements on mechanical properties and electrical conductivity.

2 Background

This chapter aims to present the fundamentals of copper processing, from ore to finished coil. Firstly, the general production route of processing copper ore to cast copper cathodes will be described. A more detailed process itself is highly demanding and thus comprise measures out of scope for this report. Secondly, the two main manufacturing processes available at Elcowire AB will be presented. They include the Vertical Upwards Continuous Cast (VUCC) process provided by Rautomead Ltd. and the Southwire Continuous Casting and Rolling (SCR®) system. Details regarding important process parameters, machine parts and manufacture routes will be described.

2.1 From Ore to Cathode

As a chalcophile element, copper ore is typically found as sulphide minerals [6] and mined ore consists of approximately 0.5 - 2% Cu. The ore must therefore be extracted and processed to achieve a high-grade concentrate. During the concentration process the copper ore particles are separated from unwanted elements and minerals. Physical processes such as crushing and grinding are used, as well as flotation techniques [7] to increase the copper amount to about 30% [1]. The copper is further extracted, firstly by the means of pyrometallurgy, which requires high-grade concentrates [6]. During smelting for copper ores containing iron, e.g., chalcopyrite ($CuFeS_2$), three phases are formed: matte, slag, and gas. Iron is oxidised, sulphur removed as gas phase SO_2, resulting in a remaining sulphide-rich copper matte and oxide-rich slag. The smelting process is essential to control the oxidation and ensure low impurity levels in the metal, such as gangue material. Gangue usually comprise of the oxides Al_2O_3, CaO, MgO and SiO_2. The slag contains most of these impurities, as well as much Fe, S, and some Cu. The immiscibility of the matte and slag promotes easier separation, where the slag can either be discarded, or cleaned and reintroduced into the smelting furnace for further metal and Cu recovery [8, 9]. Figure 2.1 presents the general process of metal extraction to produce copper cathodes.

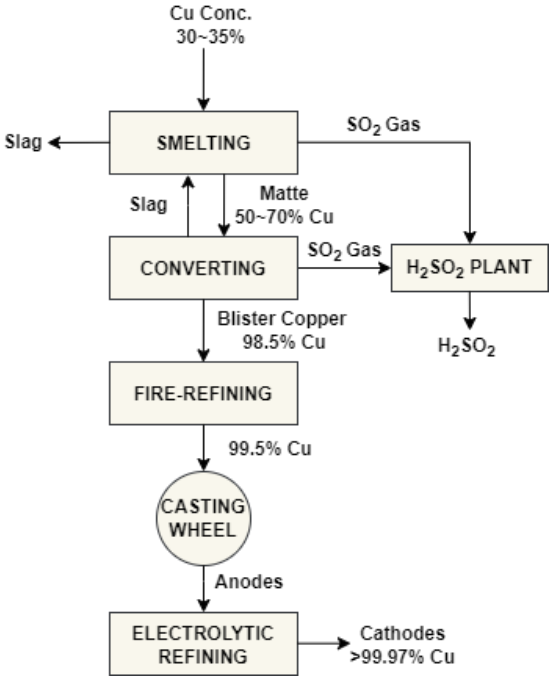

Figure 2.1. Process chart of a typical copper production process. Adapted from [8].

The copper matte is then converted to blister copper by several consecutive steps of oxidation to extract Cu and remove remaining sulphur. Produced slag from the converting process can be reintroduced into the smelting furnace for further extraction [9]. As reported by Shamsuddin and Sohn, there are numerous converting processes available. Each process consists of distinct technologies and chemical reactions, mainly depending on the copper concentrate composition [8]. Fire-refining of molten blister copper allows for further removal of oxygen and sulphur through hydrocarbon and air flow in an anode furnace. Sulphur is removed with an oxygen flow, dissolving in the melt to form SO_2, which may further be utilised in sulphuric acid (H_2SO_4) production. The deoxidation is principal to minimise copper oxide precipitation and ensure quality anode casting, where oxygen is removed as carbon dioxide and water. This accounts for oxygen left from earlier process steps and the desulphurisation [10].

The final melt is then cast as anodes, where the uniformity of the produced anodes is important for further refining. They are continuously cast where produced anode scrap can be incorporated into earlier process steps if any fault or impurities are noted [10]. Continuous electrolytic refining and electrowinning are the two major methods to produce high purity copper cathodes (> 99.97% Cu) with a controlled oxygen content. The process consists of an electrochemical cell, where Cu^{2+} ions from the anode travels through an electrolyte consisting of copper(II) sulphate ($CuSO_4$) and H_2SO_4 and plated onto a metal cathode. The copper cathode is notably low in impurities as the anode impurities are not dissolved in the electrolyte [11].

2.2 Production Processes

Rautomead Ltd. and Southwire Company are two prominent manufacturers of continuous casting machines. Their technologies are used at the production site of Elcowire AB to produce oxygen-free copper (Cu-OF) including high-copper dilute alloys and electrolytic tough-pitch (ETP) copper. Depending on the desired product, different continuous casting processes has numerous variations and are continuously modified to optimise the process and to meet customer specifications.

2.2.1 Vertical Upwards Continuous Cast (VUCC)

Metal rods can either be produced horisontally or vertically. The VUCC process is appropriate in the manufacture of Cu-OF rods due to formidable cooling flow rates, resulting in minimal defects and beneficial inner structure of the metallic Cu grains [12]. The process was developed to meet the need of 8.0 mm high conductivity Cu-OF products, including cast dilute Cu-bearing alloys. It can cast rods from 8.0 mm up to 32 mm, utilising simultaneous casting of several rods and of different diameters [13].

The main parts of a continuous cast machine model RS manufactured by Rautomead Ltd. are [14]:

i. Resistance furnace
ii. Continuous withdrawal machine
iii. Super-cooling system
iv. Control panel
v. Cathode feed system
vi. Coilers

Apart from water flow rate, other important casting parameters include e. g., casting speed, withdrawal cycle, casting die materials and temperature of the melt. These process parameters and their optimisation is vital to the microstructure and properties of the finished product. As reported by Bagherian et al., an increased casting speed, cooling rate and pulling distance resulted in finer grain structure and may also lead to earlier product fracture [14]. The general production route for a VUCC process is described in Figure 2.2. The route comprises the main parts of the process as presented above, including product testing and packing.

Figure 2.2. General procedure from start to end-product for a VUCC process. Cathodes are fed into the charging side of the resistance furnace, where they are melted by electrical heating. The melt is then cast into rods and tested before being coiled and packaged.

2.2.1.1 Resistance Furnace

The single resistance furnace with electrical heating elements includes melting, holding, and casting. Thereby no molten metal transfer is exposed and is favourable to produce an oxygen-free product. The furnace graphite crucible is depicted in Figure 2.3 and consists of two connected chambers which contain about 2400 kg of liquid melt. The charge chamber melts the automatically fed cathodes before the melt is transported to the casting chamber, connected by a base orifice of the crucible [15]. The system is lined with graphite to eliminate the risk of oxidation of the molten copper and inherently the product. This includes a filter bed consisting of graphite cubes at the base of the casting chamber [16]. The casting dies are also lined with graphite, and the integrated super-cooler draws up copper melt using vacuum to cast the melt into rods [15, 17].

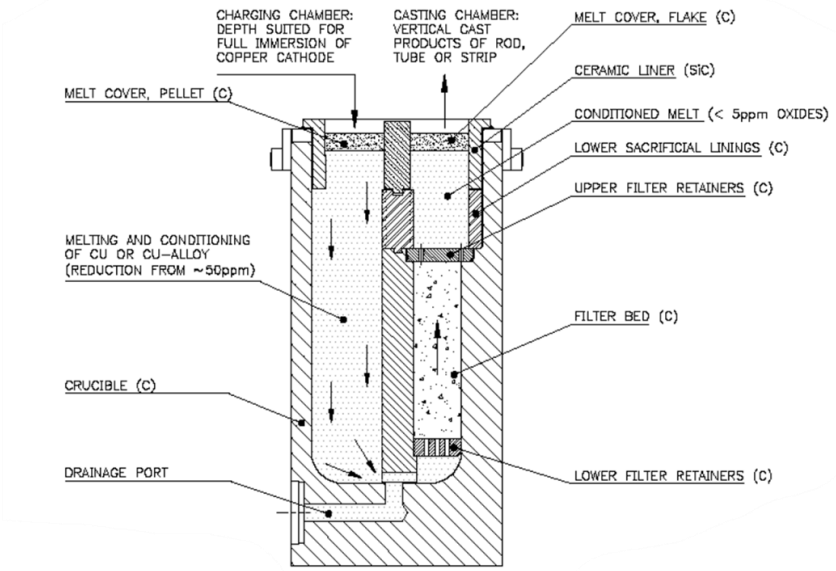

Figure 2.3. Cross-section of a graphite crucible manufactured by Rautomead Ltd. The containment system has integrated melting, alloying and oxide reduction. The 'C' denotes parts of the crucible which are graphite [13].

As graphite degrades in an oxygen-rich environment, the internal assembly of the VUCC must be in an inert gas environment, which further promotes deoxidation of the melt [18]. High-purity graphite flakes are scattered on the exposed copper melt on both the melt and cast side, protecting the melt, and acting as a reducing agent of the surface. Commonly, a flux of inert gas is similarly used to further protect the exposed copper melt and the scattered graphite flakes. Together with the inert gas environment, sacrificial linings are also used to protect the system from oxidation. Although sensitive to oxygen, graphite is highly temperature resistant. Together with its excellent electrical conductivity, it makes graphite a formidable heating material at elevated temperatures and in low voltage heating systems. The system is electrically heated at approximately 40 V, which heats the metal and controls the melt temperature by radiation and natural convection. The fluid motion of the melt is thus not externally controlled, instead the resistance heating mechanism ensures that the melt remains still in the graphite crucible for easier castability [13, 18].

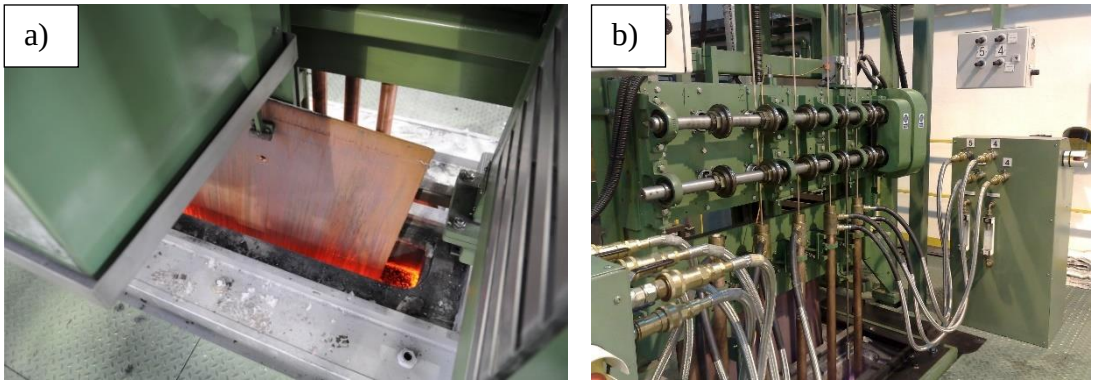

Figure 2.4. a) Melting of cathode with is automatically fed into the charging chamber of the graphite crucible b) General set-up of a withdrawal unit including coolers [19].

2.2.1.2 Addition of Magnesium

For production of oxygen-free dilute Cu-Mg alloy rods, the Rautomead Ltd. RS can be altered for specific additions of magnesium. The alloying magnesium can be introduced by the addition of weighed elemental Mg ingots wrapped in copper foil. The ingots are added at the charge side of the furnace chamber, where the fed cathodes push them into the melt chamber (see Figure 2.3). Since the ingots are added manually, this method is heavily dependent on the machine operators. Mg can also be added by an automatically fed cored wire, which consists of elemental powdered magnesium enclosed in copper. The wire is introduced lower into the melt to disperse, ensuring greater control of the melt composition and less magnesium loss. The automatic feed system is regulated with respect to the casting speed and cathode weight [13].

2.2.1.3 Super-Cooling System and Casting Dies

The super-cooling system is crucial to produce high-quality rods. The water flow rate is readily controlled to change the characteristics of the rod, such as microstructure. Recirculation of water allows for superior cooling as the copper melt is drawn upwards through graphite dies [13]. The casting dies are partially submerged in the melt, where a floater evaluates the melt level to ensure uniform immersion of each die [15]. When exiting the system, the produced rod is yet warm to the touch at an approximate temperature of 80°C. Copper is prone to oxidation and has a broad range of surface oxidation temperatures, where

higher temperatures leads to more oxidation and lower leads to nm thin oxidation films Continuously cast Cu-OF and dilute alloys have a very thin oxide layer, which is a positive feature in rod production as it increases the corrosion resistance. This further implies the need for an eminent super-cooling system [20, 21].

2.2.1.4 Withdrawal System

The withdrawal system is the determining factor of the casting speed and is positioned above the graphite dies with the integrated super-cooling system. Consisting of vacuum controlled rollers, the system draws and transports the produced rods vertically from the dies in a pulse-like manner. This is depicted in Figure 2.4.b, showing a withdrawal and super-cooling system. When producing e.g. oxygen-free Cu-Mg alloy, an electrically driven AC servo motor may instead be used [15]. Different withdrawal cycles may be applied depending on the desired product and their solidification mechanisms. For instance, higher cooling rates leads to shorter solidification times and, in turn, increases the casting speed. The casting speed is then directly dependent on the pull distance of the rod from the die. Alternating these mechanisms of pulling and solidification, implementing them as pauses and pushbacks, establish four different withdrawal cycles for the vertical continuous casting process [14, 22]. The produced rods are later tested and neatly coiled, with a maximum weight of approximately 4-5 tonnes [15]. Figure 2.5 presents a general schematic of a Rautomead Ltd. VUCC process, including four coilers.

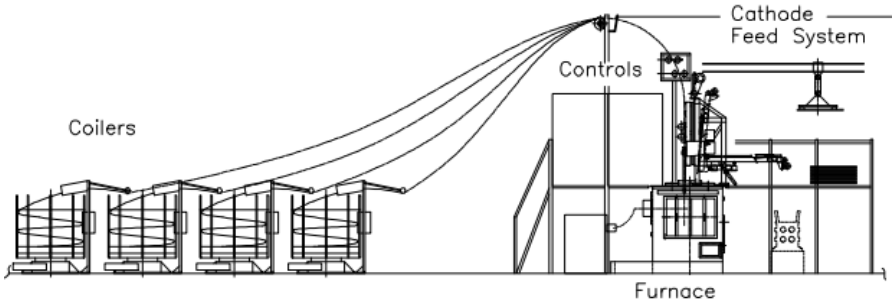

Figure 2.5. Schematic overview of a VUCC process manufactured by Rautomead Ltd. [15].

2.2.2 Southwire Continuous Casting and Rolling (SCR®)

Southwire Company provides manufacturing systems which includes continuous casting and rolling methods (SCR®) of copper rods and wires. The system is specifically used to produce ETP copper of varying diameters from 8 up to 25 mm [23]. The SCR® system is one of several available production lines for casting and rod milling, where other examples include those manufactured by Hazelett and Properzi. The Southwire SCR® technology consists of several parts, with design features developed by Southwire directly and by other contributing companies [23]. The general production route is described by Figure 2.6, and the process include the following parts:

i. Shaft furnace
ii. Furnace loading system
iii. Molten metal transportation system
iv. Holding furnace
v. Wheel-and-band casting machine
vi. Rolling mill
vii. Shearing system
viii. Coiler
ix. Electrical control system

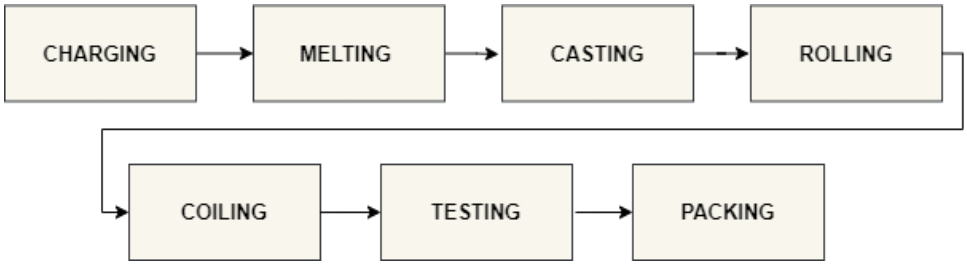

Figure 2.6. General procedure from start to end-product for a SCR® developed by Southwire. Feedstock including cathodes and various scrap are fed into the shaft furnace for melting. The melt is then cast into rods using a wheel-and band technique, then transported to the rolling mill before being coiled, tested, and packaged.

2.2.2.1 Shaft and Holding Furnace

In contrary to the VUCC process which utilises a single furnace system, the SCR® technology includes separate furnaces for charging and holding. Charge materials are loaded into a vertical shaft furnace for melting, where the solid charge moves downwards by gravity with a total capacity of 8-60 tonnes per hour. The furnace is heated with natural gas and allows for melting by the means of counterflow of the rising combustion gases. Numerous charge materials may be used, where electrolytically refined copper cathodes are commonly used to produce ETP copper. Specific for the Southwire process, up to 20% of various high-quality scrap can be loaded into the furnace. Examples include rolling mill scrap where entire faulty coils may be used, as well as other scrap alloys and Cu-bearing materials. The molten copper is then kept in a holding furnace with a capacity of 7-40 tonnes to ensure a consistent temperature and composition before being introduced to the casting machine. Slag vessels and filter beds are also incorporated into the furnace system to minimise impurities in the cast rod and wire [17, 23].

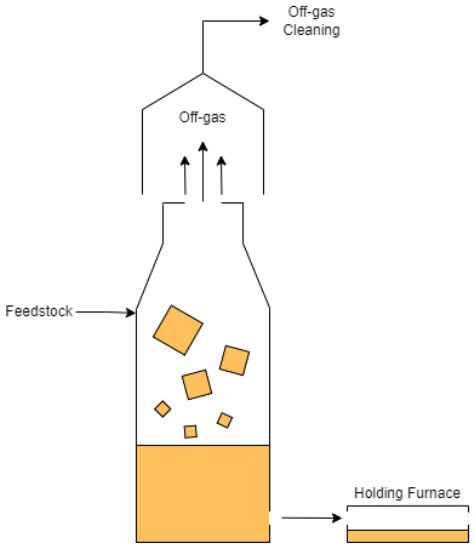

Figure 2.7. Schematic of a shaft furnace and holding furnace.

2.2.2.2 Rod Casting

For production of ETP copper rods, a wheel-and-band system is applied, as shown in Figure 2.7. The schematic depicts the rotating casting wheel with a mould integrated into its perimeter. The steel band moves coherently with the wheel and closes the mould as the molten metal is poured from the tundish. The tundish is vital for controlling the flow of molten copper into the casting process, as well as maintaining the melt temperature. The melt is then solidified with continuous spraying of cooling-water before being transported to the rolling mill by the means of an idler wheel and a bar conveyor, exiting the casting system at a temperature between 940-1015°C [17, 24].

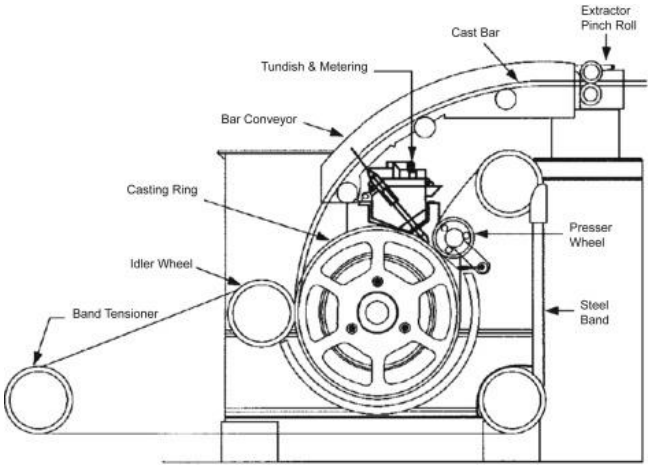

Figure 2.8. Schematic of continuous casting wheel for producing copper rod by SCR® technologies from Southwire Company [17].

2.2.2.3 Rolling Mill

From the casting wheel, the produced rod enters the rolling mill consisting of several consecutive pairs of rolls, shown as a double-roll stand in Figure 2.9. The SCR® system applies the Morgan stand mill, comprising of ten roll pairs interchangeably arranged in horizontal and vertical positions. Each roll pass is shaped in an elliptical or circular manner which, together with the alternating positions, minimises the risk of side spreading between each individual pass. This allows for easier control of the rod dimensions during rolling [25, 26]. The hot-working process is carried out above the recrystallisation temperature to deform the material and gradually reduce the rod diameter. The alloy microstructure becomes increasingly refined between each roll pass with a final grain size of approximately 20 µm [25] and contributes to a homogenous distribution of in the ETP copper. The particles are dispersed from the microstructure grain boundaries along the rolling direction, which innately changes the mechanical properties of the produced rod [27]. As the presence of Cu_2O at the grain boundaries increase brittleness, the alignment decreases the risk of ductile fracture. This increases the drawability of ETP copper to fine wires in cold-working processes [28]. After hot rolling, the surface of the produced rod is cleaned in a sequent pickling system to ensure a smooth and oxide-free surface. This is commonly done using dilute acid and is a vital step before fine wire drawing [29].

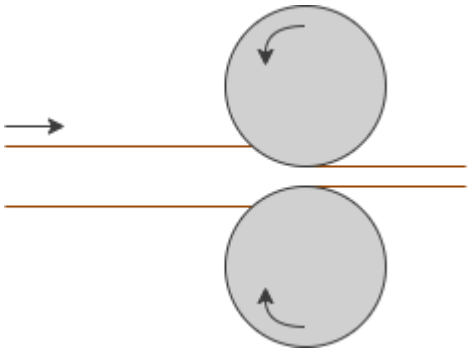

Figure 2.9. Schematic of double-roll stand. The SCR® system utilise ten alternatingly placed roll pairs to ensure greater rod dimension control.

3 Theory

This chapter will, firstly, include a presentation of the materials which are commonly used at Elcowire AB. Relevant for the VUCC process and SCR® rolling mill are copper cathodes as feedstock and Cu-bearing alloys. Material characteristics such as mechanical properties and electrical conductivity are described, as well as how the addition of alloying elements affect the product including composition and impurity limits. Furthermore, phase diagrams describing the principal material systems will be presented, followed by a brief section regarding the microstructure of cast oxygen-free coppers. Lastly, the theory of applied analytical techniques in the project are presented.

3.1 Materials

3.1.2 Copper and Dilute Copper Alloys

Copper is known for its high electrical and thermal conductivity and is readily engineered through different metallurgical techniques. The commercial importance of Cu lies in its eminent ability to be altered to fit consumer needs. Due to its high electrical conductivity, the majority of Cu is used in electrical applications, where properties such as corrosion resistance and malleability are essential [30]. The International Annealed Copper Standard (IACS) describes the electrical conductivity scale in percentage and was based on a Cu standard when first established. It is currently known that the only element with higher electrical conductivity than Cu (103% IACS) is pure silver (106% IACS) [29]. The addition of alloying elements, such as Al, Ag, Fe, Mg, Ni and Sn allow for a broad range of Cu-bearing materials and products. The properties of Cu and alloying elements used at Elcowire AB are summarised in Table 3.1. Alloying assists in enhancing specific material characteristics often related to mechanical properties such as hardness, tensile strength, and corrosion resistance. Any addition reduces the electrical conductivity, regardless of if Ag is the alloying element, as this increases the scattering of conduction electrons leading to higher resistivity. Cast Cu and Cu-bearing alloys are also ductile materials with high workability, which are easily further altered by the means of both cold- and hot metalworking processes. Rolling, drawing, billet and rod casting are examples of such, which also contribute to a change of the material properties [29, 31].

Table 3.1. Properties of Cu and the alloying elements at T = 298 K used at Elcowire AB [32].

Element	Molar Mass [g mol^{-1}]	Density (ρ) [g cm^{-3}]	T_m [°C]	T_b [°C]	Thermal Conductivity (λ) [J s^{-1} m^{-1} K^{-1}]	Electrical Conductivity (σ) [MS m^{-1}]
Cu	63.55	8.96	1085	2572	401	58
Ag	107.9	10.5	962	2212	429	63
Mg	24.31	1.74	650	1110	156	22
Sn	118.7	7.30	232	2602	67	8.7

The high workability of Cu is a result of the atomic arrangement in the metal crystal structure, where, along with other common metals, Cu has a close-packed face-centred cubic (FCC) structure. The FCC unit cell in Figure 3.1 displays the atom sites at the corners and at the face centres of the cell. The atomic density varies along different crystal directions, which gives Cu its anisotropic nature [28]. This directional dependency arrangement affects the physical properties, such as ductility and drawability, which may greatly vary depending on the

structure direction. For instance, cold- and hot working cause plastic deformation and hardens the material, affecting the present dislocations and inherently the atomic structure [33-35]. The FCC structure contains four slip planes in {111} (marked in Figure 3.1) with three possible slip directions, resulting in a total twelve possible slip systems [33]. The non-closely packed body-centred cubic structure (BCC) may contain more slip systems than FCC, where the difference in ductility lies in the atomic close packing of the crystal structures. The close packing of FCC promotes easier gliding of atomic planes in comparison to BCC structure and metals exhibiting FCC crystal structure are therefore more ductile [36]. For high-copper alloys with low alloying element contents the crystal structure remains in FCC.

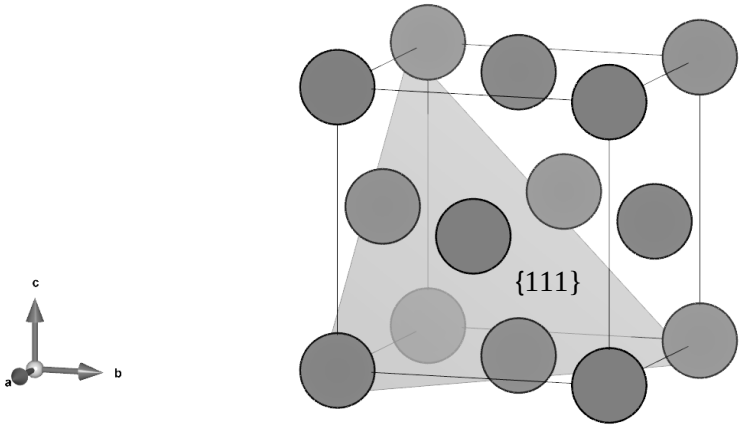

Figure 3.1. Face-Centred Cubic (FCC) unit cell in standard orientation. Atoms are placed at the corners and at the face centres of the cell. Four slip planes are present in {111}, each containing three possible slip directions [37].

3.1.2.1 Electrolytic Tough-Pitch (ETP) Copper

Electrolytic tough-pitch (ETP) copper is produced with a varying oxygen contents of 100 – 600 ppm and a minimum purity of 99.90% Cu [17]. The oxygen content is readily controlled to reach a desirable amount to guarantee proficient electrical conductivity (101% IACS). Primarily, the retained oxygen removes unwanted solute impurities by precipitating them as oxides, thus ensuring the electrical conductivity. Secondly, the oxygen forms precipitates of cuprous oxide (Cu_2O) at the grain boundaries, which makes ETP copper unfavourable in environments and applications where H_2 is present. The formation of oxides is due to the limited solubility of oxygen in solid copper, as observable in the Cu-O phase diagram (Figure 3.2). In certain heat treatment or welding processes, ETP copper with present Cu_2O may form vapor pockets which decreases the ductility and makes the product prone to fracture. Rapid cooling from melt state may lead to supersaturation and create an undesired amount of oxygen, and negatively affecting both the product in terms of ductility and production process. [28, 31]. To ensure sufficient mechanical and electrical properties, it is therefore important to maintain strict composition limits. The chemical composition of ETP copper is presented in Table 3.2 and essentially contains equivalent elemental limits as for copper cathodes and oxygen-free copper, which are further presented in Sections 3.1.2.2 and 3.1.3.

Table 3.2. Chemical composition of Electrolytic Tough-Pitch (ETP) copper according to the Swedish Standard SS-EN 13601:2021 [38].

Element	Max. Composition in ppm
Cu	- [1)]
Bi	5
O	400 [2)]
Pb	50
Other	300 [3)]

1) Including Ag, up to max. 150 ppm
2) O contents up to 600 ppm is accepted
3) The total of other elements is defined as the sum of Ag, As, Bi, Cd, Co, Cr, Fe, Mn, Ni, P, Pb, S, Sb, Se, Si, Sn, Te and Zn.

3.1.2.2 Oxygen-Free Copper (Cu-OF)

Oxygen-free copper (Cu-OF) entails a class of cast copper alloys with a strictly low oxygen content. For Cu-OF, the acceptable amount of oxygen is < 10 ppm, whilst for oxygen-free electronic (Cu-OFE) copper it is maximum 5 ppm. This means that the level of impurities in oxygen-free coppers is excessively low, with a minimum purity of 99.95% Cu. No Cu_2O particles are present in the microstructure, giving rise to high electrical conductivity (101% IACS) suitable for electrical applications with high conductive demands. Consequently, during production of Cu-OF, higher demands on the copper cathodes and a more controlled casting environment is needed [17, 29]. Manufacturing an oxygen-free product ensures that no Cu_2O is present at the grain boundaries and therefore minimises the risk of fracture in reactions and processes where H_2 is present.This increases the ductility of the product, making Cu-OF and other oxygen-free alloys suitable for e.g., drawing processes for wire and rod manufacturing [17, 31]. The chemical composition of Cu-OF is shown in Table 3.3 where the oxygen limit must conform with the standard hydrogen embrittlement requirements.

Table 3.3. Chemical composition of Oxygen-Free Copper (Cu-OF) according to the Swedish Standard SS-EN 13601:2021 [38].

Element	Max. Composition in ppm
Cu	- [1)]
Bi	5
O	- [2)]
Pb	50
Other	300 [3)]

1) Including Ag, up to max. 150 ppm
2) O contents shall agree with H embrittlement requirements (EN 1976)
3) The total of other elements is defined as the sum of Ag, As, Bi, Cd, Co, Cr, Fe, Mn, Ni, P, Pb, S, Sb, Se, Si, Sn, Te and Zn.

3.1.2.3 Copper-Magnesium (Cu-Mg)

Elcowire AB produces various oxygen-free dilute Cu-Mg alloys with a maximum of 6700 ppm Mg (0.67 wt% Mg), in accordance with Table 3.4. Very low additions of Mg results in solid solution single-phase alloys, which will be further described in Section 3.2.2. The addition of alloying Mg allows for material alterations without greatly compromising the beneficial properties of Cu. This includes high mechanical strength and preservation of the

high electrical conductivity. In a research study carried out by Strzępek and Zasadzińska, an increased Mg contents in dilute single-phase Cu-Mg alloy observably increased the hardness and tensile strength. An increase in brittleness and remarks of fractures were noted as the impact resistance decreased. This effect is explained due to magnesium having a larger atomic radius than copper (1.73 Å and 1.40 Å respectively) [39] and therefore reduces the ductility as crystal dislocations become more strained. The electrical conductivity decreases almost linearly with an increasing Mg content, with an intermittent effect below 3 wt% Mg. As Mg is a very light material, a linear density decrease is also observable [40, 41]

Table 3.4. Oxygen-free dilute Cu-Mg alloys produced at Elcowire AB with included Mg tolerances.

Alloy	Mg contents in ppm	Mg contents in wt%	Mg contents in at%	Tolerances Mg in %
CuMg0.14	1400	0.14	0.36	-0.0 / +0.06
CuMg0.22	2200	0.22	0.57	-0.02 / +0.03
CuMg0.29	2900	0.29	0.75	-0.02 / +0.04
CuMg0.42	4200	0.42	1.09	-0.04 / +0.02
CuMg0.49	4900	0.49	1.27	±0.03
CuMg0.67	6700	0.67	1.73	-0.02/+0.03

3.1.2.4 Copper-Tin (Cu-Sn)

Tin is a common alloying element in copper-bearing alloys. At 10 wt% of Sn and above, the commercial alloys are known as bronze and is commonly found with other alloying elements as ternary systems. Sn is used in dilute binary alloying material systems of Cu as well, existing as a single phase up to 1 wt% Sn. The homogenous structure makes dilute Cu-Sn readily engineered to achieve proficient mechanical properties and electrical conductivity. Compared to Mg, Sn has a larger atomic radius at 2.17 Å, further straining the crystal structure of Cu [39]. Cast Cu-Sn from 0.18 to 0.50 wt% Sn has therefore been observed to increase the material hardness with increasing Sn contents and as the microstructure becomes more refined, the overall strength of the alloy increases. Further treatments, such as severe plastic deformation, greatly contribute to this effect [42]. The negative effect on electrical conductivity of alloying with Sn is less than, for instance, Mg in solid solution systems. In Cu-Sn alloys with up to 0.4 wt% Sn, the conductivity decreases almost linearly with increasing Sn contents with an approximate value of 82% IACS at 0.3 wt% Sn [29]. The dilute oxygen-free Cu-Sn alloys manufactured at Elcowire AB are presented in Table 3.5. Elcowire AB mainly produces CuSn0.25 where other Sn contents are in consensus with the purchaser.

Table 3.5. Oxygen-free dilute Cu-Sn alloys produced at Elcowire AB with included Sn tolerances.

Alloy	Sn contents in ppm	Sn contents in wt%	Sn contents in at%	Tolerances Sn in %
CuSn0.015	150	0.015	0.008	-
CuSn0.25	2500	0.25	0.134	0.21 – 0.27
CuSn0.4	4000	0.4	0.215	-

3.1.2.5 Copper-Silver (Cu-Ag)

The general advantage of producing dilute Cu-Ag alloys is the lesser increase in electrical resistivity, inhibiting the conductive properties. Ag as alloying element has a smaller effect on the resistivity compared to Mg and Sn [29]. This allows for altering the mechanical properties with increasing Ag contents without greatly affecting the conductivity. Elcowire AB produces dilute oxygen-free Cu-Ag alloys with an Ag content up to 2000 ppm (0.20 wt%), shown in Table 3.5. The strength has been reported to increase with alloying contents and the hardness of the material as the structure dislocations become more strained due to the atomic radius of 1.72 Å of Ag[39]. The alloy furthermore becomes less prone to deformation as the creep strength increases. Cu-Ag material systems are therefore suitable in applications which require high demands in both strength and electrical conductivity, even at lower alloying contents. For additions up to 1000 ppm, Ag refines the grain structure, and the alloy will exist as a solid solution of Cu and Ag up to 8 wt% Ag before an Ag-rich phase will precipitate and form in the Cu bulk material [28, 43].

Table 3.6. Oxygen-free dilute Cu-Ag alloys produced at Elcowire AB with included Ag tolerances.

Alloy	**Ag contents in ppm**	**Ag contents in wt%**	**Ag contents in at%**	**Tolerances Ag in %**
CuAg0.01	100	0.01	0.006	0.008 – 0.012
CuAg0.03	300	0.03	0.018	0.025 – 0.035
CuAg0.04	400	0.04	0.024	0.035 – 0.045
CuAg0.10	1000	0.10	0.059	0.080 – 0.120
CuAg0.20	2000	0.20	0.118	0.180 – 0.220

3.1.3 Copper Cathode

As present oxygen must be exceedingly low in Cu-OF which requires high purity feedstock. According to the Swedish Institute of Standards (SIS), Grade A cathode feedstock (Cu-CATH-1) must therefore be very low in impurities, summarised in Table 3.7, and usually contains 60-80 ppm oxygen. The number of allowed elements are many, where the impurity limits are low to ensure the quality of the finished products. Generally, the production of Grade A cathodes results in lower impurities than those presented in Table 3.5. Especially important are the limits for Bi, Se and Te. They increase brittleness as the elements affect the grain boundaries in the microstructure and cause cracks, thus decreasing the ductility and inherently drawability of the produced rods. Other examples which increase brittleness include As, Pb and S, but the effects are not as prominent as the aforementioned elements. The presence of Fe, Cr, Si and P, among others, effect the annealability of the product [13, 17].

Table 3.7. Chemical composition of Grade A copper cathodes (Cu-CATH-1) according to Swedish Standards Institute SS EN1978:2022 [44].

Element	Max. Composition in ppm
Cu	-
Ag	25
As	5 [1)]
Bi	2
Cd	- [1)]
Co	- [3)]
Cr	- [1)]
Fe	10 [3)]
Mn	- [1)]
Ni	- [3)]
P	- [1)]
Pb	5
S	15 [4)]
Sb	4 [1)]
Se	2 [2)]
Si	- [3)]
Sn	- [3)]
Te	2 [2)]
Zn	- [3)]
Sum of elements other than Cu	65

[1)] (As + Cd + Cr + Mn + P + Sb) maximum 15 ppm
[2)] (Bi + Se + Te) maximum 3 ppm of which (Se + Te) maximum 3 ppm
[3)] (Co + Fe + Ni + Si + Sn + Zn) maximum 20 ppm
[4)] The sulphur contents shall be determined on a cast sample

3.2 Phase Diagrams

3.2.1 Copper-Oxygen (Cu-O)

The Cu-O system is distinctive regarding its phases, consisting of two condensed solid and liquid phases and additional gas-phase oxygen. The system has been investigated both theoretically and experimentally with respect to thermodynamical data and pressure stability. Described by Neumann et al. [45] and Hallstedt et al. [46], the stable intermediate phases and stoichiometric compounds cuprous oxide (Cu_2O) and cupric oxide (CuO) are present and the assumptive formation of Cu_4O_3 is considered. It has been concluded in later works that Cu_4O_3 is a metastable phase with an upper stability temperature between 400-500°C and is thereby not included in the Cu-O phase system in Figure 3.2 [47].

A liquid miscibility gap is observable in Figure 3.2 between monotectic temperatures from 1225 to 1345°C. This phase-change is described by Reaction (1) where the higher temperature details the critical point of the miscibility gap. The other observable phase-changes are represented by the monotectic and eutectic Reactions (2)-(4). Notable in the diagram is the upper stability temperature of CuO at 1278°C at higher at% O. During cooling, the gaseous and liquid phase results in the new phase CuO and this mechanism is described by a peritectic reaction. As the oxides Cu_2O and CuO exist together from 33.3 to 50 at% O, their congruent melting points are similar, 1230 and 1229°C respectively.

$$L \leftrightarrow L_1 + L_2 \text{ at } 21.5 \text{ at\% } O \text{ and } 1345\ ^\circ\mathrm{C} \tag{1}$$

$$L_2 \leftrightarrow L_1 + Cu_2O \text{ at } 31.0 \text{ at\% } O \text{ and } 1225\ ^\circ\mathrm{C} \tag{2}$$

$$L \leftrightarrow Cu_2O + CuO \text{ at } 39.0 \text{ at\% } O \text{ and } 1080\ ^\circ\mathrm{C} \tag{3}$$

$$L \leftrightarrow (Cu) + Cu_2O \text{ at } 1.70 \text{ to } 33.3 \text{ at\% } O \text{ and } 1065\ ^\circ\mathrm{C} \tag{4}$$

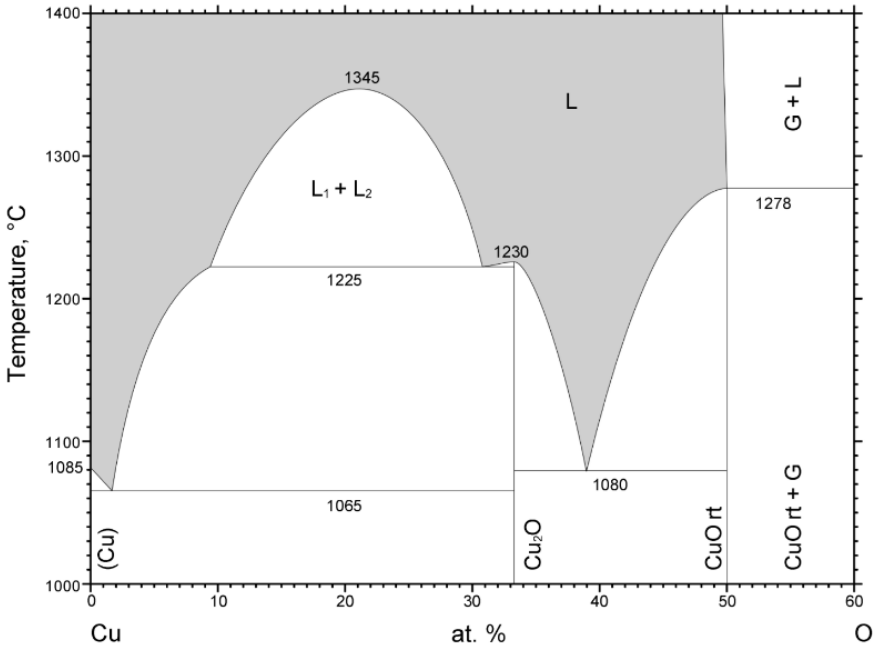

Figure 3.2. Cu-O binary phase diagram depicting a monotectic point at 31.0 at% O and two eutectic points at 33.3 and 39.0 at% O respectively. Present intermediate phases are cuprous oxide (Cu_2O) and cupric oxide (CuO) with congruent melting temperatures of 1230 and 1229°C [48].

3.2.2 Copper-Magnesium (Cu-Mg)

Several studies have been conducted regarding CuMg alloys and present phase transitions and equilibrium points, as presented by the binary phase diagram in Figure 3.3. Notable assessments of the system have been done by Nayeb-Hashemi and Clark and includes the two intermetallic compounds $MgCu_2$ and Mg_2Cu, also known as Laves phases, and three eutectic compositions shown in Reactions (5)-(7).

$$L \leftrightarrow Cu + MgCu_2 \text{ at } 21.0 \text{ at\% } Mg \text{ and } 723\ ^{\circ}\mathrm{C} \quad (5)$$

$$L \leftrightarrow MgCu_2 + Mg_2Cu \text{ at } 58.0 \text{ at\% } Mg \text{ and } 553\ ^{\circ}\mathrm{C} \quad (6)$$

$$L \leftrightarrow Mg + Mg_2Cu \text{ at } 85.0 \text{ at\% } Mg \text{ and } 485\ ^{\circ}\mathrm{C} \quad (7)$$

$MgCu_2$ is ordered in a FCC structure and is a non-stoichiometric compound, i.e., varying maximum compositions of Mg depending on the temperature. A higher temperature increases the composition range, and at stoichiometric composition the compound has a congruent melting point of 792°C. Mg_2Cu rather melts congruently at 568°C with fixed stoichiometry and is characterised by an orthorhombic crystal structure. At approximately 7 at% Mg, maximum solubility of Mg in Cu is found at the eutectic equilibrium temperature of 723°C [49, 50].

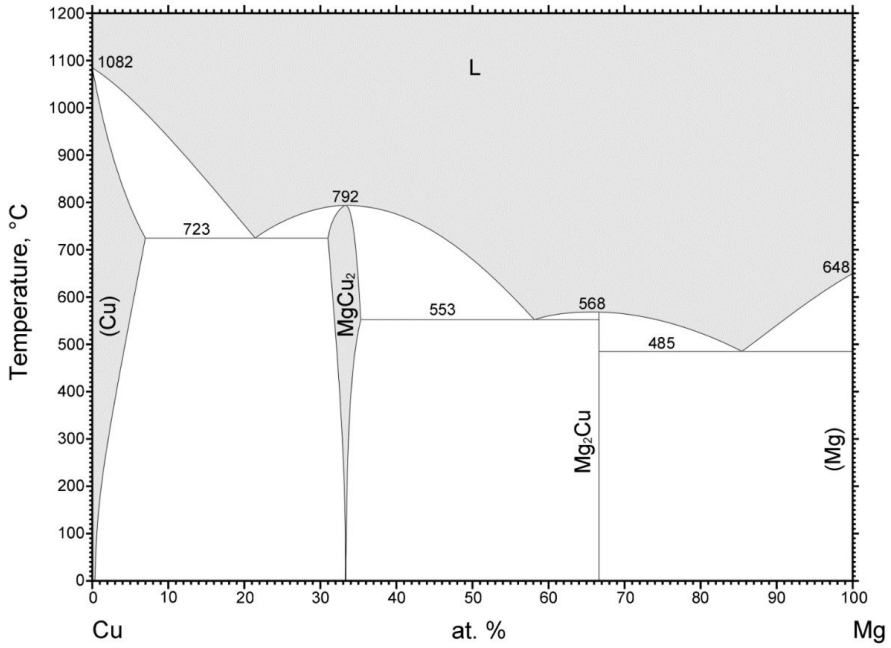

Figure 3.3. Cu-Mg binary phase diagram depicting three eutectic points at 21.0, 58.0 and 85.0 at% Mg respectively. Present intermetallic compounds and Laves phases are $MgCu_2$ and Mg_2Cu, with congruent melting temperatures of 792°C and 568°C [51].

3.2.3 Magnesium-Oxygen (Mg-O)

Notable in the Mg-O system is the lack of a solubility line. As stated by Weridt, investigations regarding the oxidation of Mg have been made where no significant results have established a clear solubility limit of O in Mg. It is, however, deemed as very low and the formation of second phase MgO is inevitable [52]. The two stable phase transformations present in the system are shown in Reaction (8) and (9). They are both melting points and exist at 0 at% O and 50 at% O respectively.

$$Mg(L) \leftrightarrow Mg(s) \text{ at } 0 \text{ at\% } O \text{ and } 650\ ^{\circ}\mathrm{C} \tag{8}$$

$$MgO(L) \leftrightarrow MgO(s)\ 50 \text{ at\% } O \text{ and } 2775\ ^{\circ}\mathrm{C} \tag{9}$$

A three-phase equilibrium of L-(Mg)-MgO is observable at a temperature of 650°C. The Mg-O system has seemingly been difficult to investigate due to insufficient thermodynamical and quantitative data. Therefore, it has not been established if mentioned equilibrium is eutectic or peritectic. Further work on the system has been carried out by Hallstedt, resulting in Figure 3.4, stating that the solubility of O in Mg is too small to be notable in the phase diagram [53]. Weridt further states that other compounds such as MgO_2, Mg_2O and MgO_4 exist. Uncertainties regarding thermodynamic data of these phases has evidently made it difficult to establish their stabilities to be included in the Mg-O phase system [52].

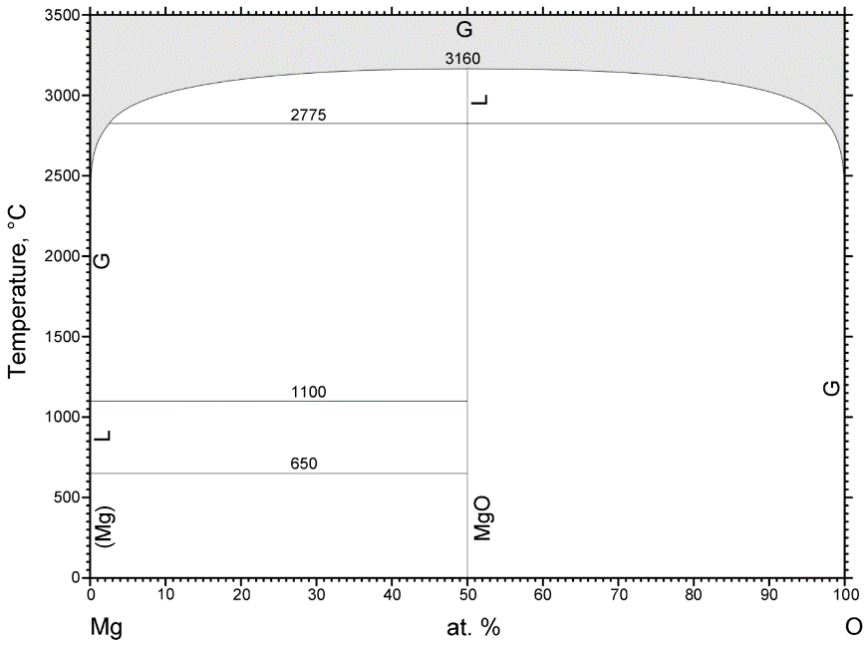

Figure 3.4. Mg-O binary phase diagram depicting two melting points at 0 and 50 at% O respectively. A three-phase equilibrium exists at 650°C but it has not been possible to establish its phase reaction. The solubility of O in Mg is very low with no apparent solubility line [54].

3.3 Microstructure of Cu-OF

The microstructure of oxygen-free coppers gives the material its eminent properties. Typical for oxygen-free alloys manufactured by the VUCC process are a combination of distinctive grains and grain boundaries. In Figure 3.5, examples of oxygen-free Cu-Mg alloy are shown to emphasise structure characteristics. Grains in the longitudinal section along the casting direction are prominent as equiaxed finer grains on the outer diameter of the rod where larger columnar grains are located near the rod axis. This is further shown in the rod cross-section where columnar grains are oriented towards the centre. Rods cast by the VUCC process shares these structure characteristics, and show greater symmetry compared to horisontal casting processes due to less gravitational influence [18, 55].

Structural differences may be altered by changing process parameters which affect grain growth. Several studies have been conducted on growth behaviour of cast metals and oxygen-free coppers. Cooling rates and casting speed are directly dependant, where these process parameters must be taken into consideration during casting to assess mechanical properties and electrical conductivity in the final product. Increasing super-cooling increases the grain growth rate and results in a finer grain structure. Smaller grains increase the hardness as grain boundaries restricts dislocations, makes the material less ductile and more prone to embrittlement as the overall strength decreases. Grains also become more homogeneously distributed with faster cooling. The super-cooling system thereby controls the cast rod solidification, where slower cooling rates allows for a larger grain size. Higher casting rates (higher cooling) increase the solidification, making the grains orientate parallel to the rod axis. Perpendicular grain orientation is instead found at lower casting speed [14, 18]. Typical for VUCC manufactured oxygen-free copper rods are grain angles of approximately 50-70° towards the rod axis [55] and smaller grains are commonly preferable to get optimal mechanical properties.

In oxygen-free Cu-Mg alloys, the precipitated Mg in the Cu bulk material acts as nucleation points for grain formation. During phase transformation from liquid melt to solid these nuclei grow, and distinctive grain boundaries are formed. Alloying content contributes to the formation of finer grains as a result of nucleation. At low additions of Mg (0.03 wt% Mg), the element has been observed to act as a grain refiner resulting in smaller and more evenly spread grains. The grain refining effect becomes less notable at even somewhat higher alloying content (0.09 wt% Mg), making the grain structure coarser [22].

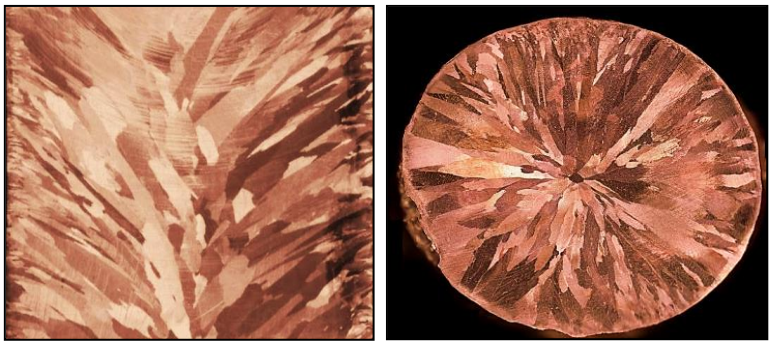

Figure 3.5. Optical microscopy images of grain structure in oxygen-free Cu-Mg alloys in vertical direction [55] and cross-section [22]. Columnar grains are found towards the rod axis, and finer equiaxed grains on the outer diameter.

3.4 Analytical Techniques

3.4.1 Scanning Electron Microscopy (SEM)

The Scanning Electron Microscope (SEM) was developed to produce magnified images of microscopic specimen features. The fundamentals were originally described in 1935 by Knoll and since then, advances in SEM technologies and analysis have made it possible to investigate physical and chemical properties of a specimen. Information regarding size and shape (topography and morphology), chemical composition and crystallography is obtainable down to a resolution of 1 nm. The microstructure may be studied to reveal information about crystal structure, grain boundaries, crystal defects and compositional variations [56].

A focused energetic electron beam is scanned across specific positions of the specimen and point by point produces a SEM image. As the electrons are accelerated to high energy and focused on a small spot, they interact with the sample and signals in the form of escaping electrons from the specimen atoms are collected. The two electron types are: (1) backscattered electrons (BSEs), generated by elastic scattering after beam and sample interaction and are higher in energy; and (2) secondary electrons (SEs), which escape close to the specimen surface due to inelastic scattering and are much lower in energy compared to BSEs. The type of electrons which are ejected is closely correlated to the resolution of the acquired SEM image where BSEs typically contribute to lower resolution images [56]. This phenomenon is described by the excitation volume, as presented in Figure 3.6.

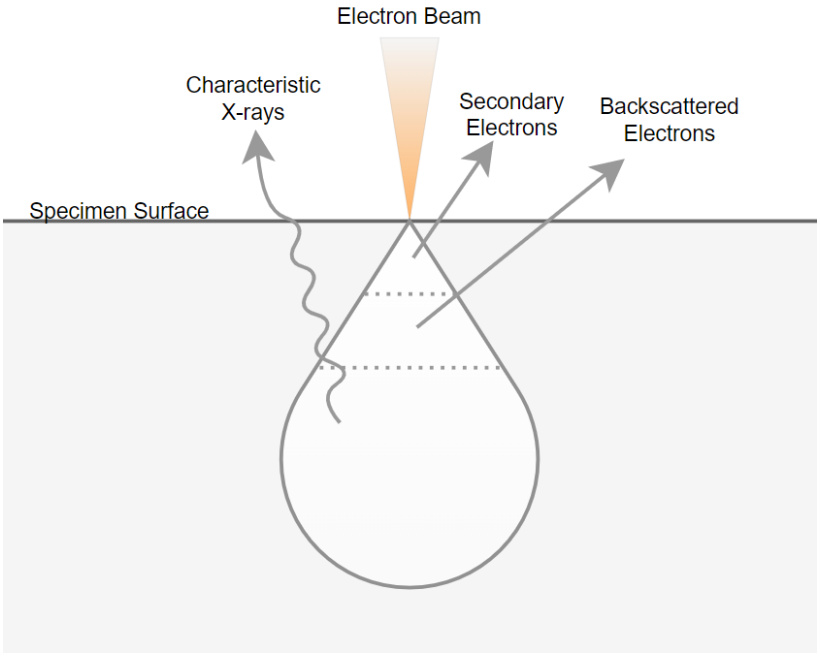

Figure 3.6. Schematic of excitation volume where a primary high-energy electron beam is scanned across the sample surface. The type of escaping electrons depends on the beam interaction and depth within the specimen. SEs escape close to the surface by inelastic scattering and BSEs by elastic scattering after beam and sample interaction. Characteristic X-rays may be collected to assess elemental information of the specimen.

3.4.2 X-Ray Energy-Dispersive Spectroscopy (XEDS)

The SEM is commonly equipped with an X-ray detector to collect produced X-rays after specimen and beam interaction. The X-rays provide qualitative and quantitative information about the specimen composition, by the means of X-Ray Energy-Dispersive Spectroscopy (XEDS). Surface atoms are excited by the electron beam and induces a vacant inner shell electron hole. Two types of X-rays are produced: (1) characteristic X-rays are emitted as the shell vacancy is filled with an electron from a higher energy state [56, 57]. Characteristic X-rays contain elemental information related to their specific energies; and (2) Continuum X-rays, which make up for the background beneath the characteristic X-ray as a result of the selected higher incident electron beam energy. Lighter elements, such as H, He and Li, do not produce X-rays and are thus not suitable for SEM/XEDS analysis The acquired XEDS spectrum include energy specific signals from the characteristic X-rays represented by intensity peaks. The intensities are directly related to the element concentration in the specimen. Considerations regarding excitation volume (see Figure 3.6), specimen X-ray absorption and additional generation of X-rays (secondary fluorescence) must be included during evaluation of the spectra [56].

3.4.3 Optical Emission Spectroscopy (OES)

Optical Emission Spectroscopy (OES) is an analytical method proficient in determining elemental composition of a sample. Numerous sample types may be analysed, where the spark OES is commonly found in the metallurgy industry for alloys and trace metal analysis. Spark OES is defined as destructive, as the spark permanently damages the sample surface. The rapid and accurate analysis makes the technique suitable for ongoing production processes to continuously assess the chemical composition. The radiation source consists of a high voltage spark, which excites the sample atoms to create a sample specific emission spectrum. When entering the optical system of the OES the emission is dispersed by grating, which splits the radiation into its monochromatic counterparts before entering the detector. The achieved spectral lines are directly proportional to the elemental concentrations [58].

4 Methodology

The following chapter presents the used analytical equipment and settings, including sample preparation methodology prior to analysis. How the data of internal scrap rates were collected and documented will be explained and principal calculations relevant to the obtained results.

4.1 Equipment

4.1.2 SEM/XEDS

The JEOL JSM-65700F SEM was provided by the Centre for Analysis and Synthesis at Lund University. The microscope is equipped with a cold field-emission gun (cold-FEG) and operated at an accelerating voltage up to 20 kV and 10 μA emission. The used detectors were lower secondary electron (LEI) detector and backscattered electron (BSE) detector. An Oxford XEDS system using a large area silicon drift detector (SDD) was used for compositional analysis. The acquired spectra were analysed using the provided AZtec software.

4.1.3 OES

An ARL^{TM} iSpark 8860 Fire Assay Analyser provided by ThermoFisher Scientific was used for composition analysis by the means of OES. The spectrometer uses an integrated photomultiplier tubes detector and Paschen-Runge optics with a one-meter focal length vacuum polychromator. The system was equipped with OXSAS^{TM} analytical software. Each sample was analysed three to ten times depending on the sample size and compared to a reference sample of known composition to determine the average elemental composition.

4.1.4 Heat Treatment Furnace

The Rohde TC 504 electrically heated heat treatment furnace was used for melting of welding wire scrap with Sn contaminants. The temperature ramp was 300°C/h to 1200°C with 15 min dwell time between each ramp. The final temperature of 1200°C was kept for 20 min before allowing the furnace and sample to cool.

4.2 Sample Preparation

4.2.1 SEM Analysis

4.2.1.1 Dross Samples

Solidified slag (dross) samples used for SEM analysis were collected in accordance with Table 4.1 during two consecutive production weeks of oxygen-free CuMg0.49 alloy rod. This was done in order to investigate the occurrence of Mg and possible oxides in the slag of the exposed melt. Samples were checked for loose graphite particles, as loose particles may harm the SEM vacuum chamber. All samples were mounted on Al-holders with a carbon film and no surface deposition was necessary prior to SEM analysis. Mounted samples used for SEM analysis are observable in Figure 4.1. The samples were collected during different production steps (mid, start and end of a production week) to assess the difference between slag samples and their compositions throughout production.

Table 4.1. Collected dross samples during the period from 22 Sep to 18 Oct. The samples were collected during either start, mid or at the end of a production week. Coil identification numbers are included for easier identification of corresponding produced coil when the samples were collected.

Sample	Production Step	Date	Coil-ID
1	Mid	22 Sep	1002348-301
2	End	23 Sep	1002348-501
3	Start	25 Sep	1002349-101
4	End	30 Sep	1002349-501
5	Start	3 Oct	1002440-101

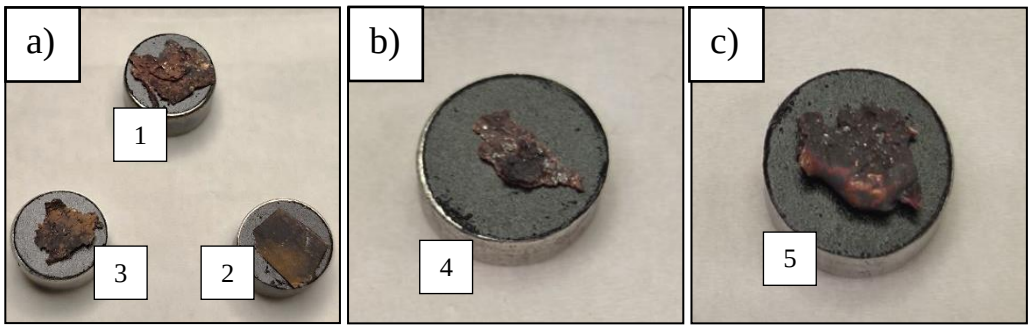

Figure 4.1. Collected dross samples for SEM analysis: a) From start, mid and end of a production week, b) Sample from production end, c) Sample from start of production week

4.2.1.2 Coil Samples

A total of seven coil samples were collected from two consecutive production batches, presented in Table 4.2, where the coil identification numbers correspond to the product batch and specific coil produced. The first seven numbers represent production batch, and the last three numbers represents the coil. For instance, as the VUCC process cast five rods simultaneously, coil-ID number 1002349-103 stands for batch 1002349, coil number one on the third coiling table. The coil samples were used for both OES and SEM analysis, where the samples did not require any preparation before OES analysis.

Table 4.2. Collected coil samples from two consecutive production batches.

Sample	Production Step	Coil-ID
1	Start	1002349-103
2	Mid	1002349-201
3	Mid	1002349-403
4	End	1002349-503
5	Start	1002440-101
6	Mid	1002440-301
7	Mid	1002440-401

The prepared sample was 30 mm oxygen-free CuMg0.49 (Sample 5 in Table 4.2). The sample was chosen due to its lower Mg contents as determined by OES. The coil sample was

analysed by the means of SEM to investigate grain boundaries and if any intermetallic phases or precipitates are present. It is of interest to evaluate how the alloying Mg is located within the sample micostructure. The objective was to compare the sample structure and phases with the consecutive samples from the same batch (Sample 6 and 7) having greater amounts of Mg. Unfortunately, due to time constraints, only Sample 5 was sufficiently prepared and used for analysis. Examples of two different coils samples are shown in Figure 4.2 including the sample which was prepared.

Figure 4.2. Examples of 30 mm CuMg0.49 coil samples before sample preparation. Some scratches from the grinding procedure are observable.

The coil sample was cut perpendicular to the casting direction into a 5.0 mm specimen by abrasive wet cutting, using an aluminum oxide cut-off wheel. The specimen surface was grinded and polished in accordance with Tables 4.3 and 4.4. The grinding was done using SiC abrasive paper with increasing paper fineness and turning the sample 90° between each step. Water was the chosen lubricant since CuMg0.49 is not water-sensitive. Several consecutive polishing steps followed using diamond paste (DP) with decreasing particle diameter and water-based DP lubricant. The last polishing step used colloidal silica as the polishing element with no lubricant necessary. All polishing steps were carried out on appropriate polishing fabric cloths with increasing abrasive fineness.

Table 4.3. Grinding steps for sample preparation of oxygen-free CuMg0.49 coil sample.

Step	**Abrasive (SiC paper)**	**Lubricant**
G1	P500	Water
G2	P800	Water
G3	P1200	Water
G4	P2000	Water
G5	P4000	Water

Table 4.4. Polishing steps for sample preparation of oxygen-free CuMg0.49 coil sample.

Step	**Abrasive**	**Lubricant**
P1	DP (3 μm)	DP Water-based
P2	DP (1 μm)	DP Water-based
P3	DP (1/4 μm)	DP Water-based
P4	Colloidal Silica (0.04 μm)	No Lubricant

4.2.2 Melting of Welding Wire Scrap

The Cu-bearing welding wire scrap with Sn contaminants were prepared and melted into ingots in accordance with Section 4.1.4. The scrap was stacked in a graphite crucible with a graphite lid to create a relatively deoxidising environment. It is important to ensure sufficient packing of the scrap pieces to minimise the risk of porosities in the sample as porosities affect the OES results negatively. The ingot was cut with an automatic cutting wheel to remove any graphite residuals and expose the Cu-surface. The cleaned surface was then used for OES analysis to determine the chemical composition of the welding wire scrap.

Figure 4.3. Graphite crucible with stacked welding wire scrap.

4.3 Data Collection

Scrap rate documentation was carried out for one month approximately, from 12th of September to 14th of October. The data collection period was limited due to process shutdown. Information was gathered from the resource planning program SAP, personal documentation during production, and in collaboration with colleagues from the logistics and production planning departments as well as machine operators. Due to inevitable documentation delay, it was challenging to link arising scrap to a specific day. It was therefore necessary to obtain information and data from different sources to make the data more comparable.

4.4 Calculations

The following formula were used to determine average composition in the melt when different feedstock sources are utilised, contributing to the contaminant contents. It is important to state the weight of charging materials and the elemental composition to establish if the impurities exceed the maximum weight percentage or ppm allowed in the final product. Equation (10) has therefore been used to ensure that charging of various scrap during ETP copper production is within range of the accepted contaminants.

$$Average\ composition_i = \frac{x_{i,1} \cdot m_1 + x_{i,2} \cdot m_2 + \ldots + x_{i,n} \cdot m_n}{m_1 + m_2 + \ldots + m_n} \qquad (10)$$

Contaminant i in feedstock number n is measured and determined to x_i, where m_n is the weight of the feedstock.

5 Results and Discussion

The results and discussion chapter will primarily focus on possibilities to decrease the investigated scrap rates. Discussions regarding suggested method feasibility are emphasised to evaluate the implementation relevance. An attempt was made to study the microstructure of oxygen-free Cu-Mg alloy, which will be presented at the end of the chapter.

5.1 Identification of Internal Scrap

The investigation of internal scrap and scrap rates were conducted on the VUCC process manufactured by Rautomead Ltd. During the investigation period, oxygen-free dilute CuMg0.49 alloy was produced with a diameter of 30 mm with an approximate production volume of 178 tonnes. As presented in Figure 5.1, the quantity of internal scrap constitutes of 16% of the total production volume, resulting in almost 30 tonnes of scrap. The majority of arising scrap comes from the process start-up phase, i.e., when the addition of Mg is done, and the produced rod is continuously tested by the means of OES to reach the desired contents of alloying Mg. As this comprises 79% of the entire scrap volume (Figure 5.1.b) it is highly relevant to decrease the start-up scrap quantity. Consequently, if the correct alloying contents is reached at an earlier stage, the amount of needed rod tests are decreased including a reduction in produced start-up scrap.

a)

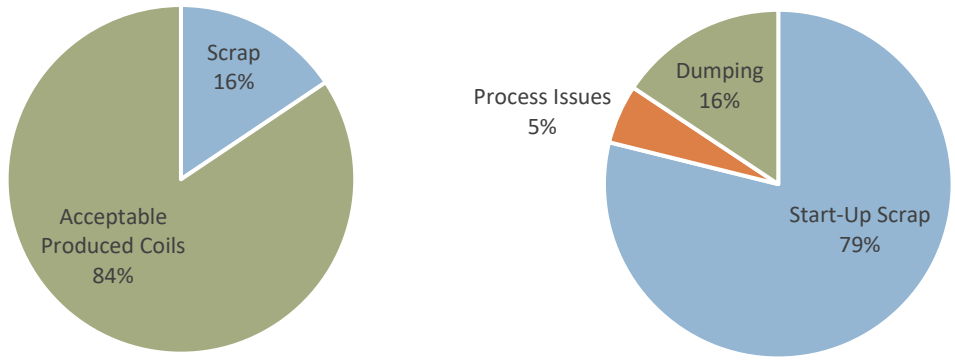

Figure 5.1. a) The internal scrap from the VUCC process corresponds to 16% out of the entire production volume. 84% are acceptable produced coils. b) The arising scrap can be classified into three groups: start-up scrap, process issue scrap and dump ingots. Most scrap (79%) comes from the start-up phase of the process.

The source of scrap varies, where, apart from the process start-up phase, scrap from process issues also contribute to the scrap rate at the level of about 5%. Different kinds of process issues are summarised in Figure 5.2, where a total of nine major complications were documented during the investigation period. The automatically controlled cathode feed system may encounter problems when cathodes become stuck during charging or when implemented sensors fail. If these issues persist for a longer time, the melt level decreases and production must be stopped, resulting in scrap as unfinished coils. The coiler tables may also face issues where the produced rods are not neatly coiled or if the rods become stuck before reaching the coiler. Problems related to the casting dies and general leakage are also relevant.

If the casting moulds are defect or not correctly connected to the super-cooling system, this results in rod failure and furthermore unfinished scrap coils.

At the end of the observed period, the VUCC process had reoccurring problems regarding limited flow between the charge and the casting chamber due to slag formation in the base orifice of the furnace. The integrated furnace filter bed is also prone to slag formation and must therefore routinely be maintained and graphite filter cubes replaced. To solve this, the furnace must be partially or entirely emptied of melt, i.e., dumped. Thus, scrap ingots are produced which may weigh up to approximately 2400 kg, which corresponds to the entirety of the furnace capacity and account for 16% of the scrap rate (Figure 5.1.b). Albeit this issue is related to the process itself, the ingots are separated from the process related issues as it is the only issue which unavoidably results in scrap as ingots and not as coils. Frequent maintenance and the control of slag formation are the sole prevention measures which can be considered to decrease the dump ingots contribution to the scrap rate. The sheer size and weight of these ingots makes them challenging to handle and there is currently no possibility to incorporate them into the VUCC process again.

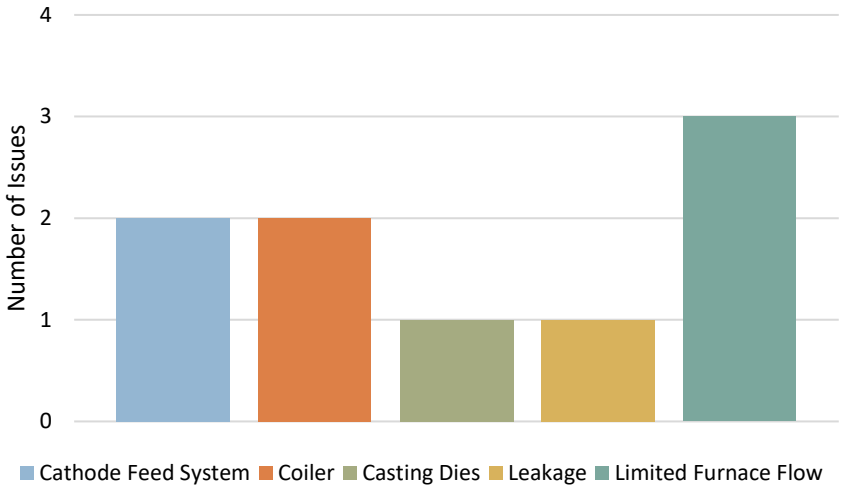

Figure 5.2. During the investigation period, nine major complications were documented. At the end of the period, the VUCC process had recurrent issues with limited furnace flow between the charge and cast side of the chamber furnace.

The majority of these issues and related produced scrap may be avoided if the problems are solved within a reasonable timeframe and with preventive measures. The main contributors to process issue related scrap are problems regarding the cathode feed system and the coilers, which may result in failure of the produced rods and thus incomplete coils. Problems with limited furnace flow are also of importance. Although slag formation in the base orifice of the furnace chamber and in the incorporated graphite filter bed are unavoidable, it is of interest to evaluate if the general slag formation of the exposed melt can be decreased which may contribute to furnace slag.

5.2 Possibilities to Decrease Scrap Rates

5.2.1 Addition of Elemental Mg by Cored Wire

As presented in Figure 5.1.b, the majority of production scrap comes from the start-up phase of the VUCC process. To decrease the time for the produced coils to meet the desired alloy

contents during the start-up phase, and thus decrease the scrap, the following method of additional addition of elemental Mg has been evaluated. The method was chosen as an alternative to the proposed procedures which will be further described in Sections 5.2.3 and 5.2.4, which requires process adapting of the VUCC or by utilising the rolling mill.

The VUCC process currently does not operate during weekends at the production site of Elcowire AB. To ensure easier start-up for the following week, the copper therefore remains in melt state in the furnace where no additional Mg is added. Due to its low density and low boiling point (see Table 3.1) the dispersed Mg is expected to rise to the top of the Cu melt and presumably contribute to slag formation of the exposed furnace melt surface. This is further discussed in Section 5.2.2 of the results. To compensate for Mg loss during production, additional 400 ppm Mg is currently added during process start-up when producing dilute Cu-Mg alloys.

To evaluate whether the start-up time and related scrap can be decreased, additional 400 ppm Mg was instead added during process shutdown at the end of a production week. This would allow for a buffer during the weekend standstill and would intuitively decrease the required amount of alloying Mg, favouring the start-up phase. 400 ppm Mg began to be added for start-up on the 26th of September and the start-up times during the investigation period are summarised in Figure 5.4. As observed, the addition of 400 ppm Mg during process shutdown seemingly did not benefit the start-up time. In fact, the start-up was longer compared to the two previous weeks when no extra Mg was added. Optimal start-up time is approximately 2-3 hours, where solely the second data point is within the preferred time range. Responsible machine operators did report shorter start-up times and no major increase in slag formation. However, conclusions regarding if the method is viable or not are difficult to interpret since at the end of the period the VUCC process had numerous complications. From the 26th of September leakage occurred and from the 3rd of October there were coiler issues, which contributed to increasing the start-up time. The following week the entire process had to be shut down due to limited furnace flow and economic reasons. Therefore, one final data point was lost in Figure 5.3.

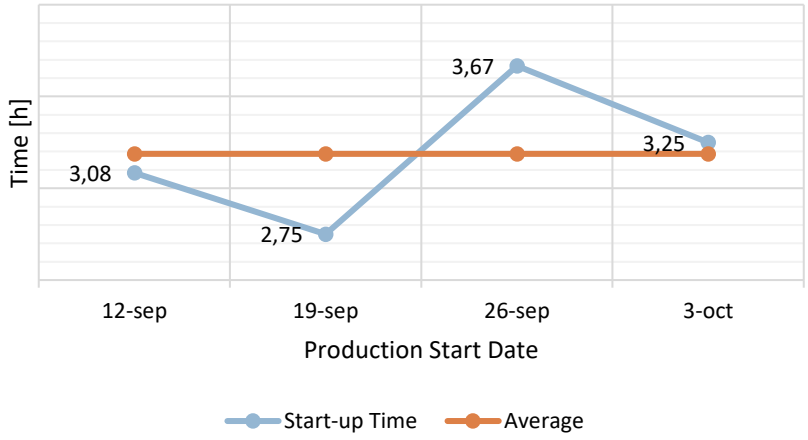

Figure 5.3. Summarised start-up times during the investigation period from the 12th of September to the 3rd of October. Additional 400 ppm Mg was added from the 26th of September and did seemingly not have a beneficial effect on the start-up time. The average start-up time was 3.19 h.

OES analysis was conducted on coil samples presented in Table 4.2 to further assess the effect of added Mg on the composition. As observable in Figure 5.4, the Mg contents greatly varied depending on when the sample was collected and analysed during production. All samples expect for Sample 4, 5 and 7 were within the allowed Mg tolerance interval presented in Table 3.4. Here, Sample 1 and 5 are the most relevant as they correspond to samples collected during production start-up after the proposed method had been applied. Sample 1 is within the accepted range whilst Sample 5 is not. It is therefore difficult to directly relate the analysed composition with the additional 400 ppm Mg. Sample 5, however, suggests that the proposed method did not have a negative effect on the produced rod, as the Mg quantity is not elevated in the overall composition.

Magnesium is thus evidently difficult to control and emphasises the need to control the melt composition. It is also important to carry out frequent analysis of the produced coils as the Mg content seemingly varies greatly depending on current production stage. Included standard deviations in Figure 5.4 furthermore indicate the difficulties to obtain definite composition values. Variances may also be due to compositional differences in the produced coil where Mg is both present in the Cu matrix and presumably at the grain boundaries. It is thus important to carry out several OES analyses over the sample surface to get an average value. An attempt was made to study the microstructure of CuMg0.49 alloy (of Sample 5) to denote such differences and will be further discussed in Section 5.3.

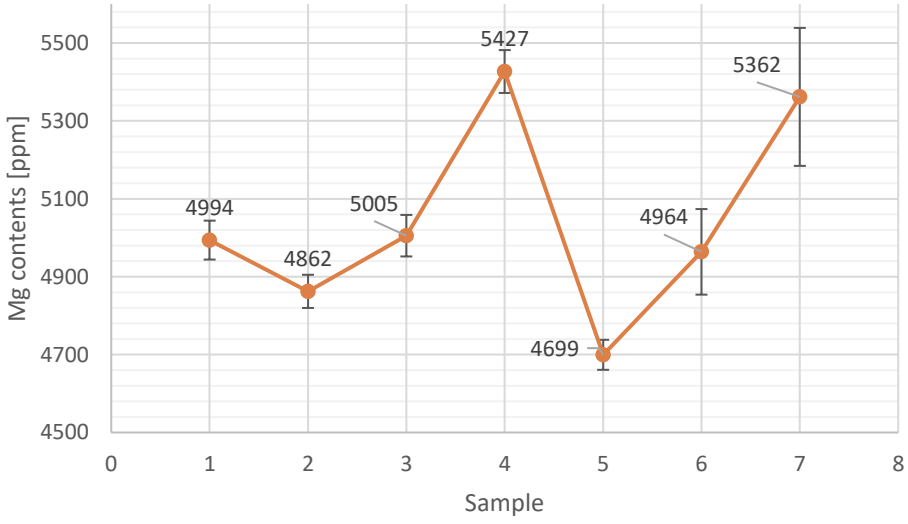

Figure 5.4. OES analysis carried out on coil samples in Table 4.2 to assess the Mg contents. All samples were collected during different production stages, where Sample 1 and 5 are from the start-up phase.

5.2.2 Control of Slag Formation

The VUCC process is described by Rautomead Ltd. as prone to slag formation during Cu-Mg casting, negatively affecting the graphite crucible and exposed melt. Rautomead Ltd. also mention that issues regarding the formation of slag is avoided in the VUCC system through the formidable design of the graphite crucible and reducing graphite flakes [55]. This statement is, however, contradictive to the observed internal scrap rates and the issues regarding limited furnace flow due to slag formation, presented in Figures 5.1 and 5.2. It is therefore relevant to investigate the prospect in how formed slag can be reduced, present elements in the slag, and which preventive measures that can be applied.

Several studies have been conducted on slag formation and minimising efforts in primary copper production processes regarding present elements, slag phases [59, 60] and metal recovery [61]. The formation of slag is evidently unavoidable, and in secondary production processes such as the VUCC, arising slag predominantly consists of oxides as stated by De Wilde et al. The study focused on the chemical losses of Cu to slag [60]. For the VUCC process during oxygen-free CuMg0.49 rod production, specifically the presence of Mg in slag is of interest. SEM/XEDS analysis was thus conducted on solidified slag samples, i.e., dross, to determine the occurrence of potential oxide phases.

Figure 5.5 presents overview images of dross Samples 1-3, presented Table 4.1 and Figure 4.1 to investigate areas of interest. The samples show apparent dissimilarity due to solidification differences. Notable areas include particle distribution observable in Figure 5.5.a and 5.5.c as well as darker areas in Figure 5.5.b. Dark regions of Sample 2 were determined to Fe and Ca deposition by XEDS point identification analysis and is seemingly contamination from sample preparation as larger dross samples had to be cut prior to SEM analysis. The presence of C, Cu, O and Mg were all detected, resulting in an initial indication of oxide formation and the dissolution of Mg from melt to slag. Specific compositions greatly varied depending on the area of analysis. Analysis was therefore conducted on samples with evident particle distribution along the sample surface.

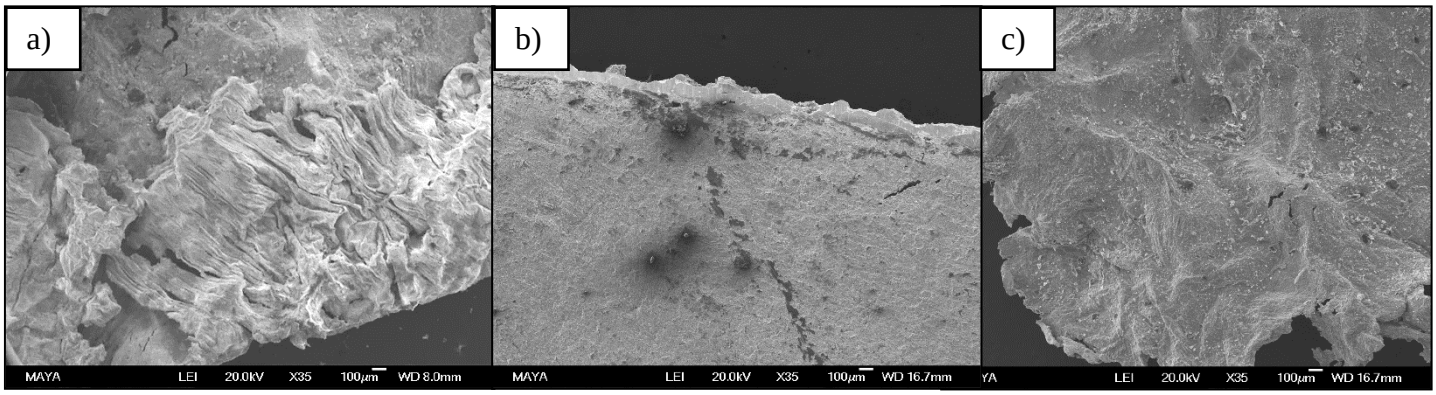

Figure 5.5. Overview SEM images of dross samples, all containing C, Cu, O and Mg. a) Sample 1, particle distribution is notable at the top of the image, b) Sample 2, darker areas were determined to be Fe and Ca by XEDS point identification seemingly deposited from sample preparation, c) Sample 3, distinct particles are observable along the entire specimen surface.

Further analysis was performed on Sample 5 (Table 4.1) to analyse distinctive surface features, as observable in Figure 5.6. The dross sample was collected during production of coil Sample 5 in Table 4.2, where a lower Mg content in the melt was detected, suggesting greater loss of Mg from melt to slag. Accumulation of carbon in the darker areas were determined by XEDS as embedded graphite flakes onto the sample surface. Pronounced particle distribution was observed Figure 5.6.c and composition analysis as chemical maps suggested the particles to consist of magnesium oxide. The maps are observable in Figure 5.7 and correspond to the surface area shown in Figure 5.6.c. The composition of the surface area measured 38 at% C, 25 at% Cu, 22 at% O and 15 at% Mg. The presence of Si was also detected but deemed insignificant due to low amounts (0.2 at% Si). Note that oxygen and carbon are lighter elements and are thus not quantified reliably. Omnipresence of certain lighter elements may skew XEDS results and must be taken into consideration as suspected contaminants. The continuous deposition of carbon from the microscope chamber onto the specimens furthermore affects quantification. The sample was moreover slightly tilted away from the X-ray detector and thus some elemental detection was lost. XEDS analysis of sample microstructure in Figure 5.6.d showed homogeneous distribution of elements, measuring to 22 at% C, 39 at% Cu and 39 at% O. Low amounts of Mg were detected (0.35 at%) but disregarded, suggesting that magnesium oxides are apparent as distinctive particles and not fully dispersed in the slag. It is thus notable that copper oxides are formed, which conforms to previous studies regarding Cu losses to slag.

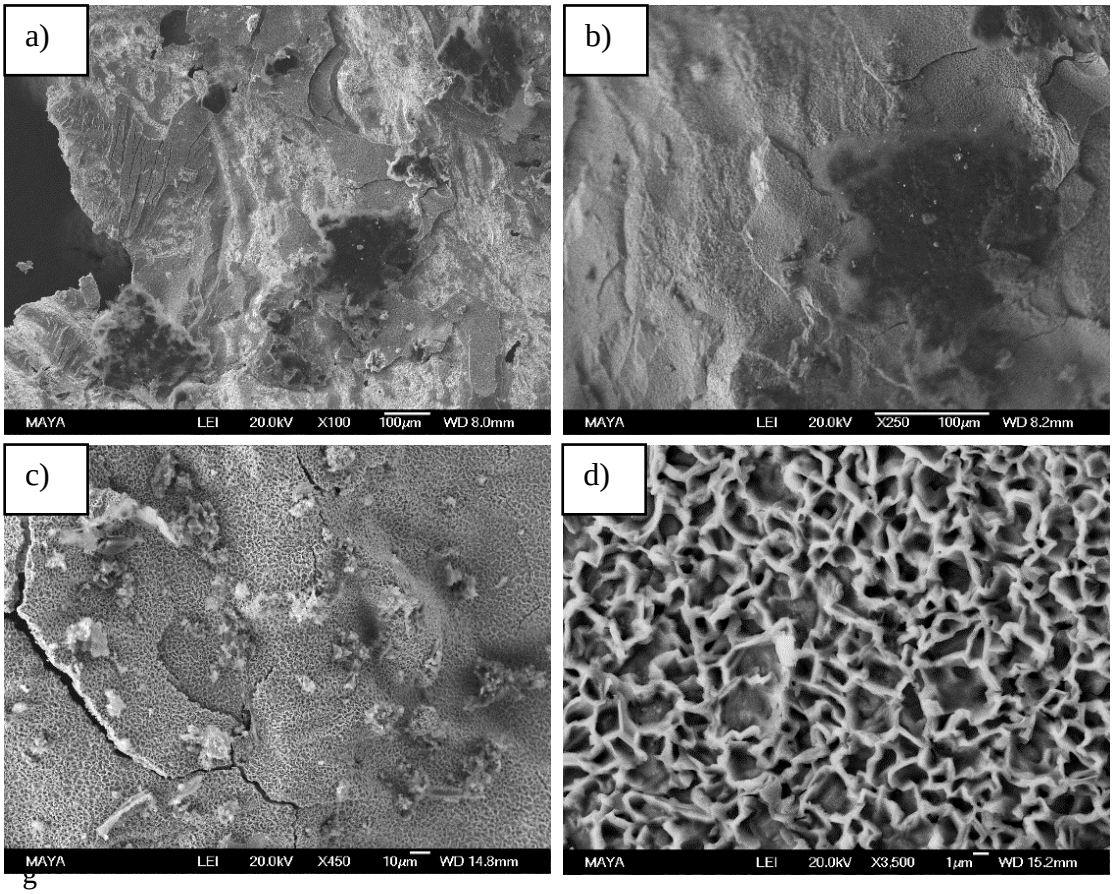

g
ure 5.6. SEM surface images of Sample 5 a) Overview image of slag structure and interesting regions, b) Graphite flakes were embedded into the slag, giving contrasting darker regions, c) Particle distribution of magnesium oxide along sample surface d) Slag microstructure.

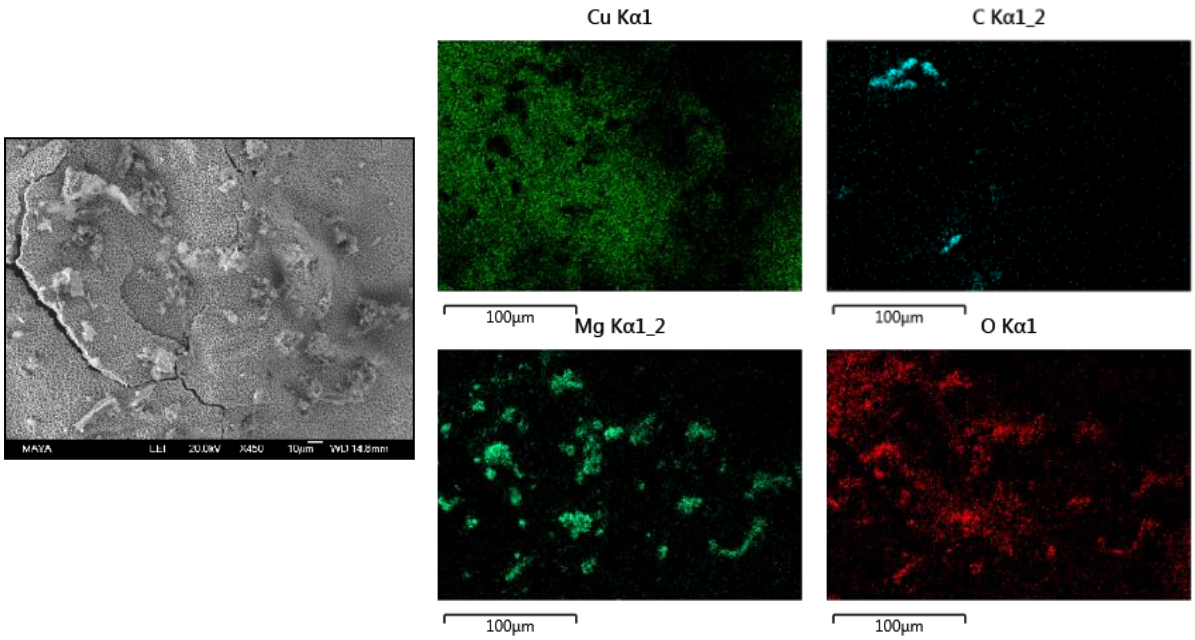

Figure 5.7. XEDS chemical maps confirming the presence of Cu, C, Mg and O in Sample 5 and their distributions. Mg and O are seemingly present as magnesium oxide particles.

Additional XEDS analysis on an oxide particle is presented in Figure 5.8. Together with the chemical maps in Figure 5.7, it is evident that Mg relates to the observed particles. The composition of the analysed particle measured to 18 at% C, 12 at% Cu, 38 at% O, 26 at% Mg, 1 at% Al and 5 at% Si. The presence of Al in the particle is questionable due to its low quantity and might be detected as a result of the sample being mounted on an Al-holder. Elements detected at low quantities might as well originate from copper cathode feedstock as contaminants. If detected elements C, Al and Si are disregarded, present elements measured to 16 at% Cu, 43 at% O and 41 at% Mg. The compositional analysis and atomic ratios suggest the presence of oxide phases MgO and CuO, where MgO is the major constituent. The presence of these oxides is further emphasised by the corresponding Mg-O and Cu-O phase diagrams presented in Figure 3.1 and 3.3, where especially O has a very low solubility in Mg leading to the unavoidable formation of a second phase.

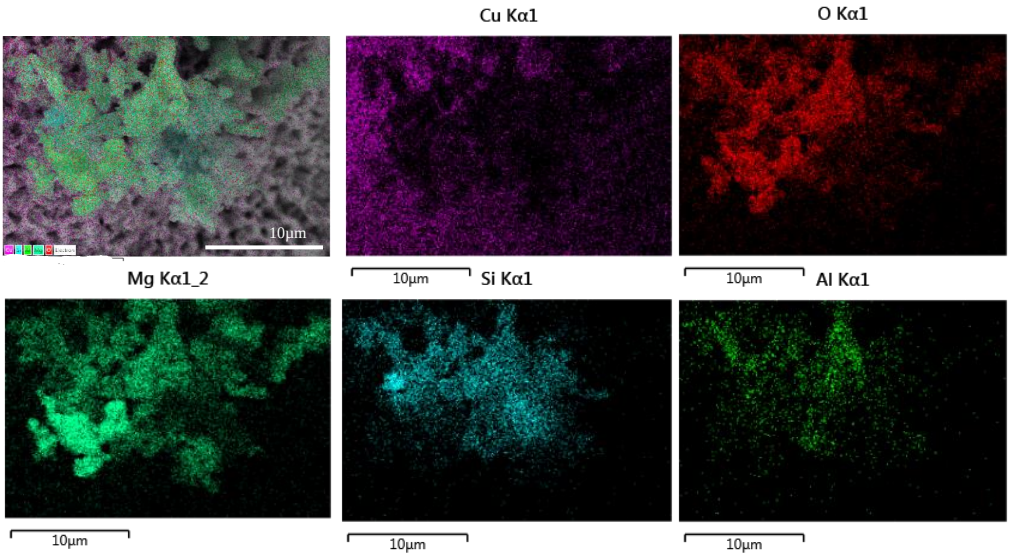

Figure 5.8. XEDS chemical maps of MgO particle in Sample 5.

During the investigation period, it was observed that the operators routinely must de-slag the exposed melt and that slag amounts greatly varied. Analysis of specific slag amounts was unfortunately hindered due to process shutdown, but further evaluation is of interest. It was nonetheless observed that the need to de-slag was unavoidable, occurring either every hour or every half hour if more slag formation was noted. The furnace holding temperature varies around 1200°C and the process operators currently utilise the method of increasing the furnace temperature by approximately 10°C to decrease slag formation. Further knowledge regarding thermochemistry and oxidation rates are needed to evaluate if this method is viable. Bagherian et al. has moreover studied the effects of increasing the melt temperature, reporting a decrease in tensile strength and easier deformation of the produced coil [22]. The presented results undoubtedly emphasise the relevance to assess new methods to ensure less oxygen absorption of the exposed Cu melt and related oxide contaminants. This would contribute to greater precision control of the allowed Mg contents during oxygen-free dilute Cu-Mg alloy production, decrease the need to de-slag and ensure adequate mechanical properties. Furthermore, it would minimise the risk of unwanted oxide non-metallic inclusions in the final product, as Mg is apparently prone to active oxidation.

Elcowire AB currently utilises an inert gas flux of N_2 to protect the graphite furnace chamber from oxidation. A N_2 flux is also used to protect the Mg cored wire which is introduced into the melt. This flux only partially protects the exposed melt of the VUCC as well, where a thick graphite layer acts as the main protectant covering the melt as a deoxidising agent. A possibility would be to replace the N_2 flux to another gas and aim to fully cover the melt. As inert gases do not partake in chemical reactions, the choice of a noble gas is seemingly appropriate. In high-temperature industrial production processes, argon gas is commonly used and also in casting processes as well [18, 62]. The calculated density of Ar (ρ = 1.78 kg m^{-3}) at standard state is higher than both air and N_2 (ρ = 1.25 kg m^{-3}) [32] meaning that argon gas would more sufficiently cover and protect the melt. Ar gas is arguably more expensive than N_2 gas, where further assessments are necessary to evaluate if the increased cost of Ar outweighs the economic loss of arising scrap rates and slag formation. Other examples of covering gases include dilute SF_6, which is commonly used in Mg refining technologies and is less expensive than Ar and N_2. SF_6 is however classified as a greenhouse gas and creates further challenges regarding compound solubility in the Cu melt and is thus not a feasible alternative as a covering gas [63].

5.2.3 Incorporation of Scrap into VUCC Process

Two major possibilities were investigated to evaluate whether the arising scrap can be repeatedly incorporated into the VUCC process. For this, considerations regarding specifically production process design and operator workloads must be performed. The produced scrap is not internally used today, but instead sent back to the cathode supplier to be recycled and cast into new copper cathodes. The first given opportunity to incorporate scrap into the VUCC process would be to directly introduce produced faulty coils into the chamber furnace to be remelted and recast as new rods. As the produced coils may vary in length depending on the reason as to why they were discarded, it is likely that most of the coils must be cut beforehand. However, as mentioned in Section 5.1, the diameter of the produced rods is 30 mm, which puts certain demands on how the coils can be handled. At the given moment, Elcowire AB does not have the capability nor capacity to continuously cut large scrap coils of this diameter into shorter manageable lengths. This would preferably require an automatic cutter to reduce the workload on the machine operators. Furthermore, the ability to add

directly scrap to the furnace chamber is limited. The area of the exposed melt on the charge side of the chamber is small and specifically constrains the operators if the scrap were to be added manually. To avoid this, inspiration can be taken from UPCAST®, Finland where they utilise automatic vibrating feed tables in their casting lines to charge scrap pieces, shown in Figure 5.9 [64]. The feed table weighs the incoming scrap pieces to ensure controlled addition to the furnace. This feature is important to maintain compositional accuracy during the production of Cu-OF and dilute oxygen-free Cu-bearing alloys. The technology, however, requires a complete redesign of the VUCC process at Elcowire AB to be able to incorporate such a feeding system, which is currently not feasible.

Figure 5.9. UPCAST®, Finland apply the technology of an automatic feeding table for their upward continuous casting machines [64].

The second method would be to utilise the technologies of the automatic wire feed presented in Section 2.2.1.2. The VUCC process manufactured by Rautomead Ltd. commonly applies this technique and is developed to ensure a steady feed of cored Mg-wire. The system can handle wires up to 21 mm diameter; thus, if process coil scrap were to be used, it must be drawn to a smaller diameter to function efficiently. If shorter scrap rods are produced it may be necessary to weld them together. Consequently, this method not only puts high demands on the automatic wire feed itself, but, yet again, on the machine operators who would be responsible for the drawing process and the mounting onto the automatic wire feed system. This method would, however, perhaps be utilised for alloy rods of smaller diameter. For instance, if scrap with higher alloying content is available it can be used in the production of rods with lower alloying content. Specifically for Cu-Mg alloys, this would then remove the need to use an automated feed of Mg cored wire.

5.2.4 Incorporation of Scrap into Rolling Mill

The proposed methods of incorporating scrap into the VUCC process to be remelt and recast has its challenges. It is therefore relevant to investigate whether the VUCC scrap can be used internally in another production process available at the site. An evaluation was conducted to assess the possibilities of using produced scrap as charge material into the rolling mill during ETP copper production. The evaluation is based on using oxygen-free CuMg0.49 as one of the main feedstock materials. It includes advantages and disadvantages as well as theoretical

calculations regarding ETP copper contamination limits. Unfortunately, the proposed method could not be put into practice.

The SCR® rolling mill is capable of using high-quality scrap as charge materials, where the main feedstock is copper cathodes. It takes approximately 3-4 hours from charging to finished ETP copper wire coil with a production rate of 30 tonnes/h. The process is currently loaded with a wide arrange of Cu-based scrap materials from both internal and external sources. The primary scrap feedstock are faulty ETP copper coils and Cu-bearing welding wire scrap contaminated with Sn of varying composition and quantities from external sources. Elcowire AB employs a priority plan when charging welding wire scrap, which was used as a guideline for the evaluation. The biggest challenge lies in controlling the elemental composition of the melt and furthermore the finished product. ETP copper has the composition limits presented in Table 3.2 and must not be exceeded to ensure adequate mechanical properties and electrical conductivity. Despite the sheer volume of the shaft furnace and the usage of an integrated holding furnace, the melt becomes concentrated in sections when loaded with scrap in too short intervals. It is therefore important to apply sufficient time intervals to avoid impurity accumulation in the melt and consequently the ETP copper.

Welding wire scrap contaminated with Sn is currently charged with a minimum of every third hour along with copper cathodes to dilute the melt. The maximum charging capacity is 10 tonnes per loading sequence, which allows for easier melt composition control. The composition of welding scrap varies and, in general, oxygen-free CuMg0.49 contains greater amounts of Mg than Sn in welding scrap. It is therefore reasonable to suggest that CuMg0.49 scrap should be loaded at smaller quantities and/or at greater time intervals and together with copper cathodes to further dilute the melt.

Theoretical outcomes were done using Equation (10) in order to investigate how the composition of ETP copper is affected by CuMg0.49 scrap feedstock, presented in Tables 5.1 – 5.3. The results entail investigation of three separate loading sequences. The charged scrap consisted of Sn contaminated welding wire scrap, CuMg0.49 of varying compositions, and cathodes at different quantities. Copper cathodes are commonly charged in bulk units with a total weight of 2.5 tonnes for each unit whilst the sack weights of welding wire may vary depending on the scrap supplier. All material compositions are based on real specification values (copper cathodes) and averaged OES analysis results (welding wire scrap and CuMg0.49). Complete composition analysis of welding wire scrap contaminated with Sn are found in Appendix.

Charge #1 constitutes of a combination of a low quantity of CuMg0.49, two cathode loads and welding wire scrap. CuMg0.49 scrap is represented by Sample 5 in Table 4.2, with approximately 4700 ppm Mg determined by OES (Figure 5.4) The estimated average composition resulted in increased values of Mg and Sn in the melt. All other elements are below maximum composition limits for ETP copper where no specific limit is given for Mg. It is notable that Fe and Sn greatly contributes to the compositional sum of elements Co, Fe, Ni, Si, Sn, Zn, exceeding the accepted total limit of 20 ppm.

As Elcowire AB commonly utilise contaminated welding wire scrap as feedstock without negatively affecting the finished ETP copper wire, it is probable that the presence of these elements is not critical. The shaft furnace operates at temperatures above 1100°C, and

although this temperature is sufficient to keep Cu in melt state, Fe has a higher melt temperature
(T_m = 1535 °C) than Cu and will thus exist as solid impurities. Fe also has a lower density (ρ = 7.86 g cm^{-3}) [32] than copper melt, meaning that the Fe impurities will rise to the top in the holding furnace and seemingly contribute to slag formation. The oxidisation of Fe and transfer to slag is commonly found in primary copper production described in Section 2.1 and furthermore in steelmaking processes [65]. The properties of Sn are presented in Table 3.1 and has a notably low melt temperature and high boiling point. Sn will thus not escape as a gaseous phase but will melt and rise to the top of the melt due to its lower density. Along with Fe, Sn is readily oxidised and reasonably end up in the slag as well, a feature which is also commonly found in primary copper production where further metal recovery from slag is needed [4].

Table 5.1. Charge #1 consists of CuMg0.49 scrap, two copper cathode units and Sn contaminated welding wire scrap.

Feedstock Source [ppm]	Source #1 CuMg0.49	Source #2 Cathode	Source #3 Cathode	Source#4 Wire Scrap	Average Composition [ppm]
Weight Feedstock [kg]	50	2500	2500	900	
Ag	13	12	13	15	13
Al	4.73	0	0	> 0.50	0.0
As	0.56	> 0.5	> 0.50	0.67	0.50
Au	> 0.50	0.80	0.80	> 0.50	0.70
Be	0	0	0	> 0.50	0.00
Bi	> 0.50	0	0	0.38	0.10
Cd	0	> 0.50	> 0.50	0	0.10
Co	> 0.50	> 0.50	> 0.50	> 0.50	0.10
Cr	> 0.50	> 0.50	> 0.50	> 0.50	0.10
Fe	1.7	2.0	2.0	12	3.5
Mg	4700	0	0	0	40
Mn	0	> 0.50	> 0.50	> 0.50	0.20
Ni	1.9	> 0.50	1.0	> 0.50	1.0
P	1.9	0.80	0.80	> 0.50	0.70
Pb	0.63	1.0	1.0	> 0.50	0.90
S	5.2	2.3	3.3	3.6	2.9
Sb	> 0.50	> 0.50	0.60	1.4	0.60
Se	5.9	> 0.50	> 0.50	> 0.50	0.50
Si	0	> 0.50	> 0.50	> 0.50	0.50
Sn	> 0.50	1.5	1.5	120	20
Te	0.96	0.20	> 0.50	0	0.20
Zn	0	1.0	1.0	> 0.50	0.80
Zr	0	0	0	0	0

Charge #2 consists of copper cathodes as the main feedstock material and with a small quantity of 4700 ppm Cu-Mg scrap. Mg is as predicted the only present impurity with a slightly lower quantity compared to Table 5.1. The main restriction of this feedstock load is the packing on the materials. As aforementioned, the maximum capacity is 10 tonnes per charging sequence, deeming it reasonable to use additional cathodes to further dilute the melt. This is, however, restricted by the packing of the feedstock as the charging elevator can only

fit maximum three cathode units. The weight of CuMg0.49 was also varied between 25 – 200 kg, where the average composition of Mg in the melt increased proportionally with the scrap weight. It is difficult to predetermine what the maximum scrap quantity is as this depends on the oxidation of Mg and transfer to the slag. In the VUCC process, approximately 400 ppm Mg is lost and must be compensated for. If the same argument is applied during ETP copper production, a maximum of 700 kg CuMg0.49 can be utilised in a single charging sequence whilst ascertaining no other elements are above their permitted levels and maintaining a purity of 99.90% Cu. Arguably, more Mg will be lost to slag in the rolling mill due to larger areas of melt being exposed. However, if larger quantities copper cathodes and CuMg0.49 scrap are used, the operators must maintain sufficient packing of the feedstock to ensure that no material becomes stuck during charging.

Table 5.2. Charge #2 consists of CuMg0.49 scrap and copper cathodes. The scrap quantity was varied to investigate how the Mg contents was affected. This showed a proportional relationship between scrap and Mg in the final melt.

Feedstock Source [ppm]	**Source #1 CuMg0.49**	**Source #2 Cathode**	**Source #3 Cathode**	**Source#4 Cathode**	**Average Composition [ppm]**
Weight Feedstock [kg]	50	2500	2500	2500	
Ag	13	12	13	14	13
Al	4.7	0	0	0	0
As	0.56	> 0.5	> 0.50	0.50	0.50
Au	> 0.50	0.80	0.80	0.80	0.80
Be	0	0	0	0	0
Bi	> 0.50	0	0	0	0
Cd	0	> 0.50	> 0.50	> 0.50	0.10
Co	> 0.50	> 0.50	> 0.50	> 0.50	0.10
Cr	> 0.50	> 0.50	> 0.50	> 0.50	0.10
Fe	1.7	2.0	2.0	1.0	1.7
Mg	4700	0	0	0	31
Mn	0	> 0.50	> 0.50	> 0.50	0.20
Ni	1.9	> 0.50	1.0	0.60	0.70
P	1.9	0.80	0.80	0.70	0.80
Pb	0.63	1.0	1.0	1	1.0
S	5.2	2.3	3.3	2.8	2.8
Sb	> 0.50	> 0.50	0.60	> 0.50	0.50
Se	5.9	> 0.50	> 0.50	0.50	0.50
Si	0	> 0.50	> 0.50	0.50	0.50
Sn	> 0.50	1.5	1.5	1.5	1.5
Te	0.96	> 0.50	> 0.50	> 0.50	0.20
Zn	0	1.0	1.0	1	1.0
Zr	0	0	0	0	0

The feedstock for Charge #3 is similar to Charge #1, where the same quantity of cathodes is loaded but the compositions of CuMg0.49 and welding wire scrap has been changed. Note that the weight of charged welding scrap is less, as the weight varies depending on the supplier. It is also notable that the Sn contents is almost halved in comparison to Table 5.1. In turn, no other contaminant than Mg exceeds the permitted compositional values of ETP copper. The average composition for Mg is also somewhat higher due to an increased Mg

contents in the CuMg0.49 rod scrap. As observable in Figure 5.4, the Mg contents may vary depending on during which production stage the composition analysis was carried out. If greater quantities of Mg scrap pieces were to be used it would become increasingly difficult to predetermine and assess the Mg contents in the melt and furthermore finished ETP copper wire. It is therefore important to have in mind that the Mg contents in the scrap rods varies along its length. Thus, it is reasonable to prioritise VUCC start-up scrap where the Mg contents is expected to be somewhat lower.

Table 5.3. Charge #3 utilises CuMg0.49 scrap with an increased Mg contents and welding wire scrap with lower Sn contents.

Feedstock Source [ppm]	Source #1 CuMg0.49	Source #2 Cathode	Source #3 Cathode	Source#4 Wire Scrap	Average Composition [ppm]
Weight Feedstock [kg]	50	2500	2500	665	
Ag	16	12	13	15	13
Al	4.0	0	0	> 0.50	0.0
As	9.8	> 0.5	> 0.50	0.67	0.52
Au	> 0.50	0.80	0.80	> 0.50	0.72
Be	0	0	0	> 0.50	0.01
Bi	0.75	0	0	> 0.50	0.03
Cd	0	> 0.50	> 0.50	0	0.09
Co	> 0.50	> 0.50	> 0.50	> 0.50	0.11
Cr	> 0.50	> 0.50	> 0.50	> 0.50	0.10
Fe	1.7	2.0	2.0	16.	3.7
Mg	4994	0	0	0	43
Mn	0	> 0.50	> 0.50	> 0.50	0.18
Ni	2.1	> 0.50	1.0	1.2	0.77
P	1.9	0.80	0.80	> 0.50	0.73
Pb	0.67	1.0	1.0	> 0.50	0.92
S	5.3	2.3	3.3	2.9	2.8
Sb	0.65	> 0.50	0.60	0.70	0.52
Se	3.8	> 0.50	> 0.50	> 0.50	0.47
Si	0	> 0.50	> 0.50	0.68	0.52
Sn	> 0.50	1.5	1.5	70	9.5
Te	0.7	0.20	> 0.50	0.54	0.24
Zn	0	1.0	1.0	0	0.87
Zr	0	0	0	> 0.50	0

The proposed method comes with its advantages and disadvantages. The main advantage is that the need to send internal scrap back to the cathode supplier is diminished. The method principally intends to make use of the entirety of the arising CuMg0.49 scrap and can be applied to additional dilute Cu-Mg scrap of various Mg amounts. This would consequently lead to reduced strain of internal logistics and a reduction in shipping costs. It can also be presumed that the need of cathodes will decrease, including the enclosed purchasing costs. As shown in Section 5.2.2 and due to the elements low boiling point, Mg will transfer to slag and also be removed as a gaseous phase. This increases the feasibility of the suggested method as the Mg contents will be more readily maintained.

Disadvantages include those previously presented in Section 5.2.3, where specifically the large diameter makes the produced rods difficult to manage. The CuMg0.49 coils must be cut into sufficiently small lengths with relatively low weights to ensure dilution of Mg into the melt. It is thus questionable if adequate quantities of CuMg0.49 scrap can be used to outweigh the current scrap rates. The presented outcomes in Table 5.1-5.3 does, however, evidently show that the Mg contents is the main limiting factor. Although the calculations are a great method to predetermine the melt composition, it is important to take some factors into consideration. This includes the distribution of elements in the melt, impurity oxidation and transfer of impurities from melt to slag. It is also reasonable to assume that the contribution of Mg to slag formation in the rolling mill will affect the overall process as it will require additional maintenance. Remaining Mg may increase the brittleness of the produced ETP copper, making it more susceptible to wire fracture. After the method has been applied to the rolling mill, further analysis is required to determine how the product is affected in terms of mechanical and electrical properties. The proposed method will in turn require more frequent testing to ensure product quality.

5.3 CuMg0.49 Microstructure

The microstructure of Sample 5 presented in Table 4.2 was analysed by the means of SEM to investigate compositional attributes such as grain boundaries, precipitates and where the alloying Mg is located in the coil sample. The goal was to firstly identify a triple junction of grain boundaries and then analyse inside and around a specific grain. SEM microscopy is suitable to assess topography and chemical characteristics. Compositional images are commonly done by detecting signals in the form of backscattered electrons escaping from a greater depth of the sample. To optimise the number of generated BSEs, a higher accelerating voltage is required, longer dwell times and a short working distance, i.e., distance from sample to detector. A short working distance is favourable to allow greater collection of escaping BSEs. BSE imaging using the SEM microscope presented in Section 4.1.2 requires a maximum of 8.0 mm working distance.

Unfortunately, the movement of the sample within the microscope chamber became restricted at working distances below 9.0 mm and would not allow for distances below 7.5 mm. This significantly hindered the analysis and imaging as signals were lost. For Figure 5.10, 20 kV accelerating voltage was used and a working distance of 9.0 mm. Figure 5.10.a shows abrasive marks on the sample surface as a result from sample preparation. Darker spots were observed and firstly regarded as porosities, however XEDS point identification determined them to Si inclusions, presumably originating from the final polishing step of sample preparation. The small inclusions are marked in Figure 5.10.b and appear as darker spots as the lower atomic number of Si compared to Cu contributes to the contrast. A sufficient compositional BSE image could not be retrieved to assess the presence and distribution of Mg and was not related to the darker regions and spots observed in Figure 5.10.a. Any distinctive grain boundaries could furthermore not be found.

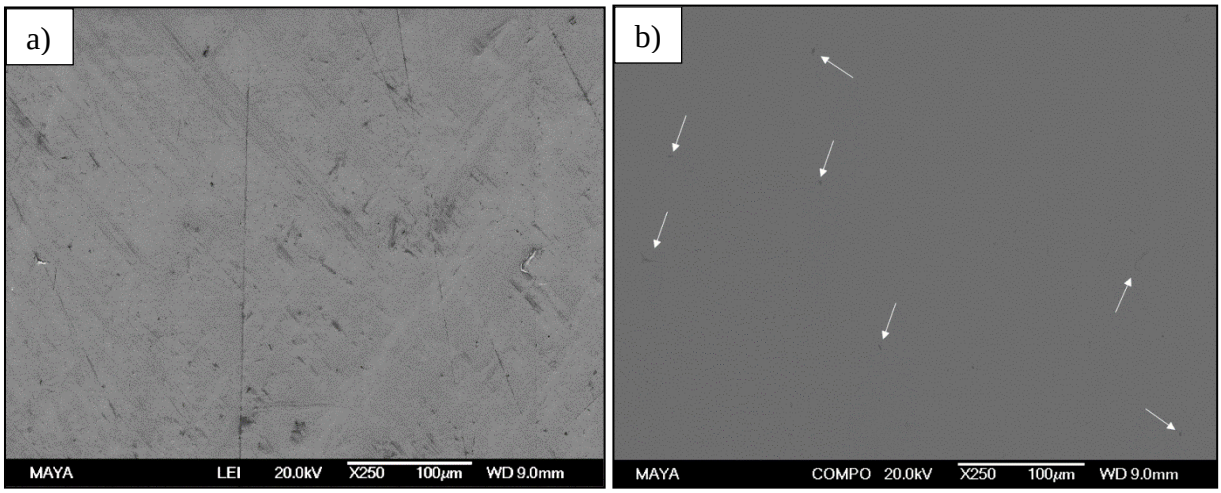

Figure 5.10. SEM images of Sample 5, oxygen-free CuMg0.49: a) Abrasive marks from sample preparation were observed using SE imaging. Darker spots were determined to Si inclusions by XEDS, b) Marked Si inclusions in BSE imaging to assess compositional differences.

XEDS analysis was carried out at several different positions along the sample surface, but no Mg was detected. According to the Cu-Mg phase diagram in Figure 3.3, the intermetallic phase $MgCu_2$ should be present even at low alloying content. The sample is presumably too homogeneous to observe any distinctive compositional differences. Arguably, it would be possible to distinguish grain boundaries through Electron Channeling Contrast Imaging (ECCI). This SEM technique is commonly used to observe dislocation density where BSE intensity is highly correlated to the crystal planes [66]. Adequate microscope settings were seemingly used to optimise BSE signals, instead imaging was restricted by microscope limitations.

6 Conclusions

The primary goal of this thesis was to identify the internal scrap rates from the Vertical Upwards Continuous Casting (VUCC) process, investigate measures regarding recyclability and suggest methods to decrease the scrap rate. The main focus was on utilising oxygen-free Cu-Mg scrap containing 4900 ppm, where suggested possibilities can be employed to other dilute Cu-bearing alloys. The internal scrap rate accounted for 16% of the total monthly production volume, resulting in approximately 30 tonnes of CuMg0.49 scrap. Primarily the produced scrap is a result of the start-up phase of the VUCC process, where large quantities of produced alloy coils are discarded due to insufficient Mg content. Other contributors to produced scrap are process related issues, resulting in unfinished coils and dump ingots from furnace emptying due to slag formation. The dump ingots cannot be readily recycled due to their sheer weight and size. It is therefore relevant to assess appropriate methods to control the Mg content to minimise start-up scrap as well as the reusability of scrap coils.

Possibilities to decrease scrap rates begins with evaluating the current production scheme of dilute Cu-Mg alloys. The VUCC process currently does not operate during weekends, thus leaving the copper in melt state and allowing for significant Mg loss. The proposed method entailed adding an extra 400 ppm Mg before weekend standstill to function as a buffer to shorten process start-up times and inherently minimise start-up scrap. The method did not have any notable positive effects on neither the start-up time nor the produced scrap. It was, however, difficult to draw any clear conclusions due to recurring process issues and the decision to shut down the VUCC process hindered subsequent analysis. Further investigation is therefore of interest to evaluate the viability of the proposed method.

The Mg content in the produced coils were shown to vary, depending on the current production stage when the coil sample was collected and analysed. The addition of an extra 400 ppm Mg did not affect the coil composition. The compositional analysis further emphasises the need to control the loss and content of Mg in the melt. Solidified slag samples were therefore analysed by the means of SEM and XEDS to investigate present oxide phases and the presence of Mg in slag originating from the VUCC process. Distinctive MgO particles were observed on the dross surfaces as well as notable Cu losses to slag. To further limit the oxygen solubility in the exposed copper melt, it is relevant to utilise an inert gas flux, such as Ar gas, to complement the already existing graphite flake layer and more sufficiently protect the melt.

Scrap recyclability may be increased by remelting produced scrap in either the VUCC process or the SCR® rolling mill. Incorporation of scrap into the rolling mill is more relevant than in the VUCC process. Produced Cu-Mg rods are difficult to handle and there are currently no apparent methods to utilise the scrap in the VUCC process without redesigning the process or by greatly affecting the responsible machine operators. If the process were to be redesigned, inspiration can be taken from UPCAST® where they utilise automatic feeding tables to charge the casting furnace with scrap. Regarding the rolling mill, the alloying Mg in the oxygen-free produced rods are the main limiting factor. It is important to avoid concentration of contaminants in the shaft furnace and take slag formation into account due to the oxidation of present impurities. Thus, oxygen-free Cu-Mg scrap must be charged in smaller quantities and preferably using scrap with lower amounts of Mg and at sufficient time intervals. The time intervals should reasonably not subceed the current interval applied for charging of welding

wire scrap contaminated with Sn. Arguably, the method can be applied to different scrap alloys and is a formidable method to predict melt composition.

Lastly, an attempt was made to study the microstructure of CuMg0.49 alloy. The cross-section sample was studied in the SEM to observe grain boundaries, potential phases, and the compositional differences regarding Mg distribution. The analysis was limited by microscope restrictions and plausibly due to the homogeneity of the sample. Grain boundaries, however, should be able to be imaged by the means of ECCI due to dislocation at the boundaries. The compositional differences observed in the BSE images were solely Si inclusions originating from the sample preparation.

7 Future Work

The presented results show great possibilities to further assess the proposed methods in terms of internal scrap rates and recyclability. Economic feasibility and viability were out of scope for this project, but future considerations are of importance. This includes an evaluation if current operating shifts may be changed to minimise produced start-up scrap. In general, a longer investigation and data collection period would allow for clearer conclusions to be drawn. This is specifically relevant to Section 5.2.1, where additional Mg was added to the VUCC process.

Regarding using produced scrap into the rolling mill, future actions would include small scale melting of scrap from the VUCC process at different scrap ratios, as similarly done in Section 4.2.2 when welding wire scrap was melted. The average composition of the ingots can then be determined by OES and compared to the presented theoretical calculations. Although sample preparation would be laboursome, small scale melting is an important first step before charging scrap feedstock into the shaft furnace. Further studies may also be carried out on other types of scrap with different alloying elements and lower contents. Analysis of the contaminants effect on the mechanical and conductive properties are also of interest.

More elaborate studies regarding slag formation in both the VUCC process and rolling mill are also needed. The formation of slag is evidently unavoidable in continuous casting processes. If an Ar gas flux is applied to the VUCC process to protect the exposed melt its effectiveness must be evaluated. This can be done in a similar manner as presented in this report, but also with other analytical techniques, such as X-ray diffraction analysis (XRD) and X-ray fluorescence analysis (XRF). These techniques are commonly used for elemental composition and phase determination in metallurgical slag from primary production processes. Many studies have been conducted of primary production and can act as guidelines for secondary production processes.

It is also of interest to investigate whether produced scrap from the rolling mill can be incorporated into the VUCC process to decrease overall scrap rates. Produced ETP copper wires are smaller in diameter, making them more manageable. The elevated oxygen content in ETP copper must then be considered as well as how the charging of scrap will be performed. Reasonably the same method presented in the results of incorporating scrap into the rolling mill can be applied.

8 References

1. ICSG. *The World Copper Factbook* 2021 [cited 2022 October 4]; Available from: https://icsg.org/wp-content/uploads/2021/11/ICSG-Factbook-2021.pdf.
2. Schlesinger, M.E., Sole, K.C., Davenport, W.G., and Alvear Flores, G.R.F., 2022, *Chapter 17 - Collection and processing of recycled copper*, in *Extractive Metallurgy of Copper (Sixth Edition)*, Elsevier. p. 467-82.
3. CA. *Copper Recycling*. 2022 [cited 2022 28 September]; Available from: https://copperalliance.org/resource/copper-recycling/.
4. Schlesinger, M.E., Sole, K.C., Davenport, W.G., and Alvear Flores, G.R.F., 2022, *Chapter 18 - Chemical metallurgy of copper recycling*, in *Extractive Metallurgy of Copper (Sixth Edition)*, Elsevier. p. 483-91.
5. Elcowire. *Our Commitments - Sustainability* 2022 [cited 2022 November 16]; Available from: https://elcowire.com/our-commitments/sustainability/.
6. Souza, R., Queiroz, C., Brant, J., and Brocchi, E., 2019, *Pyrometallurgical processing of a low copper content concentrate based on a thermodynamic assessment.* Minerals Engineering. **130**: p. 156-64.
7. Schlesinger, M.E., Sole, K.C., Davenport, W.G., and Alvear Flores, G.R.F., 2022, *Chapter 3 - Production of high copper concentrates—comminution and flotation* in *Extractive Metallurgy of Copper (Sixth Edition)*, Elsevier. p. 31-66.
8. Shamsuddin, M. and Sohn, H.Y., 2019, *Constitutive Topics in Physical Chemistry of High-Temperature Nonferrous Metallurgy—A Review: Part 1. Sulfide Roasting and Smelting.* JOM. **71**(9): p. 3253-65.
9. Schlesinger, M.E., Sole, K.C., Davenport, W.G., and Alvear Flores, G.R.F., 2022, *Chapter 4 - Pyrometallurgical processing of copper concentrates*, in *Extractive Metallurgy of Copper (Sixth Edition)*, Elsevier. p. 67-93.
10. Schlesinger, M.E., Sole, K.C., Davenport, W.G., and Alvear Flores, G.R.F., 2022, *Chapter 12 - Fire refining (S and O removal) and anode casting*, in *Extractive Metallurgy of Copper (Sixth Edition)*, Schlesinger, Sole, Davenport, and Alvear Flores, Editors, Elsevier. p. 313-29.
11. Schlesinger, M.E., Sole, K.C., Davenport, W.G., and Alvear Flores, G.R.F., 2022, *Chapter 13 - Electrolytic refining*, in *Extractive Metallurgy of Copper (Sixth Edition)*, Elsevier. p. 331-59.
12. Jones, T.D.A., Strachan, R.I., Mackie, D.M., Cooper, M., Frame, B., and Vorstius, J.B., 2021, *Computational fluid dynamic simulations of solidification for enhancing speed of continuous cast copper.* Engineering Science and Technology, an International Journal. **24**(1): p. 92-104.
13. Nairn, M., *Rautomead Technology for Continuous Casting of Oxygen-Free Copper, Copper-Magnesium & Other Copper Conductor Alloys* 2014: Rautomead International Limited, Dundee, U.K.
14. Bagherian, E.-R., Fan, Y., Cooper, M., Frame, B., and Abdolvand, A., 2016, *Effect of water flow rate, casting speed, alloying elements and pull distance on tensile strength, elongation percentage and microstructure of continuous cast copper alloys.* Metall. Res. Technol. **113**(3): p. 308.
15. Cochrane, R.S. and Nairn, M., *The Rautomead Upwards Vertical Continous Casting Process*. 1996: Rautomead International Limited, Dundee, U.K.
16. Nairn, M., *Graphite-Based Technology in Continuous Casting of Re-Draw Rod for Multi-Wire Drawing Machines*, in *Copper Wire Rod Process*. 2001: Rautomead International Limited. Scotland, UK.
17. Schlesinger, M.E., Sole, K.C., Davenport, W.G., and Alvear Flores, G.R.F., 2022, *Chapter 19 - Melting and casting*, in *Extractive Metallurgy of Copper (Sixth Edition)*, Elsevier. p. 493-509.
18. Bagherian, E.-R., *To Enable the Processing of New Complex High Performance Alloys by Improving the Capacity and Performance of Continuous Casting Equipment*. 2017.
19. Rautomead, *Rautomead Image Gallery*. 2022.

20. Aromaa, J., Kekkonen, M., Mousapour, M., Jokilaakso, A., and Lundström, M., 2021, *The Oxidation of Copper in Air at Temperatures up to 100 °C.* Corrosion and Materials Degradation. **2**(4): p. 625-40.
21. Castrejón-Sánchez, V., Coyopol Solís, A., López, R., Encarnación-Gomez, C., Morales, F., Soriano Vargas. O, Edmundo Mastache, J., and Villa Sánchez, G., 2019, *Thermal Oxidation of Copper Over a Broad Temperature Range: Towards the Formation of Cupric Oxide (CuO).* Materials Research Express. **6**(7).
22. Bagherian, E.-R., Fan, Y., Cooper, M., Frame, B., and Abdolvand, A., 2016, *Effect of melt temperature, cleanout cycle, continuous casting direction (horizontal / vertical) and super-cooler size on tensile strength, elongation percentage and microstructure of continuous cast copper alloys.* Metall. Res. Technol. **113**(5): p. 502.
23. Southwire. *Southwire Copper Rod Systems*. 2022 [cited 2022 November 14]; Available from: https://www.southwire.com/scr-technologies/scr-copper-rod-systems.
24. Shihab, N., Enab, T., Galal, A., and Ghattas, M., 2016, *Effect of Grain Size on Orange Peel in Oxygen Free Copper Wire Produced by Upcast.* International Journal of Scientific and Engineering Research. **7**: p. 1271-75.
25. Liu, Y., Peng, Y., and Qu, X., 2021, *Mechanism of and Key Technologies for Copper Bonding in the Hot Rolling of SCR Continuous Casting and Rolling.* Applied Sciences. **11**(22): p. 11023.
26. Wright, R.N., 2016, *Chapter 17 - Redraw Rod Production*, in *Wire Technology (Second Edition)*, Wright, Editor, Butterworth-Heinemann: Oxford. p. 263-70.
27. Cochrane, S., Yeoman, G., *Cu-OF or Cu-ETP: Some General Comparisons of Small Diameter Copper Wire Products* 2006: Conticast Group.
28. Wright, R.N., 2016, *Chapter 13 - Relevant Aspects of Copper and Copper Alloy Metallurgy*, in *Wire Technology (Second Edition)*, Wright, Editor, Butterworth-Heinemann: Oxford. p. 177-200.
29. Davies, J.R., 2001, *ASM Specialty Handbook - Copper and Copper Alloys*. Ohio: ASM International. p. 3-4, 15, 69.
30. Schlesinger, M.E., Sole, K.C., Davenport, W.G., and Alvear Flores, G.R.F., 2022, *Chapter 2 - Production and use*, in *Extractive Metallurgy of Copper (Sixth Edition)*, Elsevier. p. 19-30.
31. Caron, R.N., 2001, *Copper Alloys: Properties and Applications*, in *Encyclopedia of Materials: Science and Technology*, Buschow, Cahn, Flemings, Ilschner, Kramer, Mahajan, and Veyssière, Editors, Elsevier: Oxford. p. 1665-68.
32. Blackman, A.G., Gahan, L. R., 2014, *Aylward and Findlay's SI chemical data*. 7th ed., Milton, Australia: John Wiley & Sons Australia, Ltd. p. 14-20.
33. Hull, D. and Bacon, D.J., 2011, *Chapter 5 - Dislocations in Face-centered Cubic Metals*, in *Introduction to Dislocations (Fifth Edition)*, Hull and Bacon, Editors, Butterworth-Heinemann: Oxford. p. 85-107.
34. Wright, R.N., 2016, *Chapter 11 - Mechanical Properties of Wire and Related Testing*, in *Wire Technology (Second Edition)*, Wright, Editor, Butterworth-Heinemann: Oxford. p. 129-57.
35. Hull, D. and Bacon, D.J., 2011, *Chapter 1 - Defects in Crystals*, in *Introduction to Dislocations (Fifth Edition)*, Hull and Bacon, Editors, Butterworth-Heinemann: Oxford. p. 1-20.
36. Lim, S.J. and Huh, H., 2022, *Ductile fracture behavior of BCC and FCC metals at a wide range of strain rates.* International Journal of Impact Engineering. **159**: p. 104050.
37. Momma, K. and Izumi, F., 2011, *VESTA 3 for three-dimensional visualization of crystal, volumetric and morphology data.* Journal of Applied Crystallography. **44**(6): p. 1272-76.
38. SIS, *Copper and Copper alloys - Copper Rod, Bar and Wire for General Electrical Purposes*, in *SS-EN 13601:2021*. 2022, Swedish Standard Institute: Stockholm.
39. Bondi, A., 1964, *van der Waals Volumes and Radii.* The Journal of Physical Chemistry. **68**(3): p. 441-51.
40. Strzępek, P., Zasadzińska, M., *Pure Alloy Additive or Preliminary Alloy: A Comparative Study on Obtaining High-Strength Copper Magnesium Alloys Designed for Electrical Power Systems*. Energies, 2022. **15**, DOI: 10.3390/en15062093.

41. Hiekkanen, I., Renfors, T., *Oxygen-free copper alloy and method for its manufacture and use of copper alloy*, OY, Editor. 2003: Finland.
42. Ebrahimi, M., Shaeri, M.H., Gode, C., Armoon, H., and Shamsborhan, M., 2019, *The synergistic effect of dilute alloying and nanostructuring of copper on the improvement of mechanical and tribological response.* Composites Part B: Engineering. **164**: p. 508-16.
43. Felicia, D.M., Rochiem, R., and Laia, S.M., 2018, *The effect of silver (Ag) addition to mechanical and electrical properties of copper alloy (Cu) casting product.* AIP Conference Proceedings. **1945**(1).
44. SIS, *Copper and Copper Alloys - Copper Cathodes*, in *SS-EN 1978:2022*. 2022, Swedish Standards Institute: Stockholm.
45. Neumann, J.P., Zhong, T., and Chang, Y.A., 1984, *The Cu−O (Copper-Oxygen) system.* Bulletin of Alloy Phase Diagrams. **5**(2): p. 136-40.
46. Hallstedt, B., Risold, D., and Gauckler, L.J., 1994, *Thermodynamic assessment of the copper-oxygen system.* Journal of Phase Equilibria. **15**(5): p. 483-99.
47. Blobaum, K.J., Van Heerden, D., Wagner, A.J., Fairbrother, D.H., and Weihs, T.P., 2003, *Sputter-deposition and characterization of paramelaconite.* Journal of Materials Research. **18**(7): p. 1535-42.
48. *Cu-O Binary Phase Diagram 0-60 at.% O: Datasheet from "PAULING FILE Multinaries Edition – 2012" in SpringerMaterials (https://materials.springer.com/isp/phase-diagram/docs/c_0100125)*, Villars and Okamoto, Editors., Springer-Verlag Berlin Heidelberg & Material Phases Data System (MPDS), Switzerland & National Institute for Materials Science (NIMS), Japan.
49. Nayeb-Hashemi, A.A. and Clark, J.B., 1984, *The Cu-Mg (Copper-Magnesium) system.* Bulletin of Alloy Phase Diagrams. **5**(1): p. 36-43.
50. El Karim, Y., Grosu, Y., Faik, A., and Lbibb, R., 2019, *Investigation of magnesium-copper eutectic alloys with high thermal conductivity as a new PCM for latent heat thermal energy storage at intermediate-high temperature.* Journal of Energy Storage. **26**: p. 100974.
51. *Cu-Mg Binary Phase Diagram 0-100 at.% Mg: Datasheet from "PAULING FILE Multinaries Edition – 2012" in SpringerMaterials (https://materials.springer.com/isp/phase-diagram/docs/c_0904741)*, Villars and Okamoto, Editors., Springer-Verlag Berlin Heidelberg & Material Phases Data System (MPDS), Switzerland & National Institute for Materials Science (NIMS), Japan.
52. Wriedt, H.A., 1987, *The Mg−O (Magnesium-Oxygen) system.* Bulletin of Alloy Phase Diagrams. **8**(3): p. 227-33.
53. Hallstedt, B., 1993, *The Magnesium — Oxygen system.* Calphad. **17**(3): p. 281-86.
54. *Mg-O Binary Phase Diagram 0-100 at.% O: Datasheet from "PAULING FILE Multinaries Edition – 2012" in SpringerMaterials (https://materials.springer.com/isp/phase-diagram/docs/c_0907811)*, Villars and Okamoto, Editors., Springer-Verlag Berlin Heidelberg & Material Phases Data System (MPDS), Switzerland & National Institute for Materials Science (NIMS), Japan.
55. Nairn, M., *Continuous Casting of Copper Magnesium Conductor Alloys*. 2013: Rautomead International Limited, Dundee, U.K.
56. Goldstein, I.J., Newbury, E.D., Michael, R.J., Ritchie, W.M.N., Scott, J.J.H., and Joy, C.D., 2018, *Scanning Electron Microscopy and X-Ray Microanalysis*. 4th ed.: Springer New York, NY. p. 7-10.
57. Neikov, O.D. and Yefimov, N.A., 2019, *Chapter 1 - Powder Characterization and Testing*, in *Handbook of Non-Ferrous Metal Powders (Second Edition)*, Neikov, Naboychenko, and Yefimov, Editors, Elsevier: Oxford. p. 3-62.
58. Nosheen, S., Nouman, M., Habib, F., Soomro, B., Waseem, B., and Akram, M., 2020, *Comparative study of spark-optical emission spectroscopy and x-ray fluorescence spectroscopy for quantitative analysis of ferrous and non-ferrous alloys.* International Journal of Science and Research Archive. **1**: p. 51-55.
59. Isaksson, J., Vikström, T., Lennartsson, A., and Samuelsson, C., 2021, *Influence of Process Parameters on Copper Content in Reduced Iron Silicate Slag in a Settling Furnace.* Metals. **11**(6): p. 992.

60. De Wilde, E., Bellemans, I., Campforts, M., Guo, M., Vanmeensel, K., Blanpain, B., Moelans, N., and Verbeken, K., 2017, *Study of the Effect of Spinel Composition on Metallic Copper Losses in Slags.* Journal of Sustainable Metallurgy. **3**(2): p. 416-27.
61. Tian, H., Guo, Z., Pan, J., Zhu, D., Yang, C., Xue, Y., Li, S., and Wang, D., 2021, *Comprehensive review on metallurgical recycling and cleaning of copper slag.* Resources, Conservation and Recycling. **168**: p. 105366.
62. Ten, E. and Badmazhapova, I., 2013, *Obtaining high-quality cast billets from Cu-Mg alloys.* Russian Journal of Non-Ferrous Metals. **54**.
63. Bell, S., Davis, B., Javaid, A., and Essadiqi, E., 2006, *Final Report on Refining Technologies of Magnesium.*
64. Upcast. *Green Perspective - Casting High-Conductivity Oxygen-Free Copper Rod From Scrap: Myths and Reality*. 2022 [cited 2022 December 7]; Available from: https://upcast.com/green-perspective/.
65. Basu, S., Lahiri, A.K., and Seetharaman, S., 2008, *Activity of Iron Oxide in Steelmaking Slag.* Metallurgical and Materials Transactions B. **39**(3): p. 447-56.
66. L'Hôte, G., Lafond, C., Steyer, P., Deschanel, S., Douillard, T., Langlois, C., and Cazottes, S., 2019, *Rotational-Electron Channeling Contrast Imaging analysis of dislocation structure in fatigued copper single crystal.* Scripta Materialia. **162**: p. 103-07.

9 Appendix

Table A1. Sample 1, Composition OES analysis of welding wire scrap contaminated with Sn. Note that Fe content must be compared with ETP copper reference sample. Real Fe content is thus somewhat lower.

Element									**Average Composition**
Cu (%)	99.987	99.984	99.985	99.982	99.983	99.982	99.987	99.985	99.984
Ag	13.1	14.7	13.7	16.5	15.7	17.2	13.1	14.6	14.8
As	0.66	0.89	0.64	0.96	0.85	0.82	0.16	0.37	0.67
Bi	0.21	0.43	0.49	0.34	0.47	0.49	0.23	0.37	0.38
Fe	11.8	11.8	11.9	11.7	12.4	11.7	12.8	12.9	12.1
Pb	0.30	0.30	0.42	0.30	0.30	0.30	0.30	0.30	0.32
Sb	1.32	1.96	1.26	1.56	2.10	1.47	0.54	0.73	1.37
Se	0	0.22	0.30	0.29	0.13	0.02	0	0	0.12
Te	0.80	0.91	0.72	0.50	0.74	0.50	0.50	0.50	0.65
Sn	95.9	122	117	143	125	145	96.5	116	120
Ni	2.49	2.49	2.58	2.33	2.34	2.31	2.59	2.63	2.47
S	2.73	3.52	3.68	4.16	3.82	4.43	2.77	3.60	3.59
Zn	0	0	0.40	0	0	0	0	0	0.05
Al	0	0	0.01	0	0	0	0	0	0
P	0.09	0.20	0.16	0.14	0.02	0.01	0	0	0.08
Si	0	0	0.10	0	0.96	0	0.10	1.04	0.28
Mn	0	0	0	0.01	0	0	0	0	0
Cd	0	0	0	0	0	0	0	0	0
Cr	0.08	0.12	0.12	0.11	0.17	0.11	0.05	0.08	0.11
Be	0.07	0.07	0.07	0.07	0.07	0.06	0.06	0.06	0.07
Mg	0	0	0	0	0	0	0	0	0
Co	0.05	0.10	0.15	0.08	0.11	0.05	0	0	0.07
Zr	0.10	0.16	0.10	0.11	0.06	0	0	0	0.07
Au	0.22	0.22	0.25	0.24	0.17	0.08	0.05	0.04	0.16

Table A2. Sample 2, Composition OES analysis of welding wire scrap contaminated with Sn. Note that Fe content must be compared with ETP copper reference sample. Real Fe content is thus somewhat lower.

Element							Average Composition
Cu (%)	99.989	99.988	99.989	99.990	99.987	99.990	**99.990**
Ag	15.9	15.9	15.4	13.8	15.9	14.2	**14.4**
As	0.30	0.27	0.30	0.25	0.56	0.30	**0.30**
Bi	0.20	0.22	0.20	0.20	0.20	0.20	**0.20**
Fe	17.5	17.7	17.8	17.2	17.2	17.7	**16.9**
Pb	0.30	0.30	0.30	0.30	0.30	0.30	**0.30**
Sb	0.75	0.66	0.20	1.36	1.69	0.20	**0.01**
Se	0	0	0	0.06	0.02	0	**0**
Te	0.50	0.50	0.50	0.54	0.72	0.50	**0.50**
Sn	74.5	72.1	70.7	62.1	84.4	62.1	**63.4**
Ni	1.24	1.10	1.08	1.12	1.23	1.22	**1.17**
S	2.62	3.36	2.85	2.82	3.73	2.49	**2.80**
Zn	0	0	0	0	0	0	**0**
Al	0	0.23	0.25	0	0	0	**0**
P	0	0.12	0	0.16	0.14	0.03	**0.03**
Si	0	3.52	1.03	0	0.20	0	**0.02**
Mn	0	0	0.02	0.01	0.02	0	**0**
Cd	0	0	0	0	0	0	**0**
Cr	0.03	0.09	0.06	0.07	0.07	0.03	**0.05**
Be	0.06	0.07	0.06	0.07	0.07	0.06	**0.07**
Mg	0	0.02	0.01	0	0.01	0	**0**
Co	0.07	0.21	0.11	0.23	0.17	0.06	**0.10**
Zr	0	0.08	0	0.11	0.08	0	**0**
Au	0.03	0.26	0.13	0.22	0.27	0.10	**0.26**

Table A3. Sample 3, Composition OES analysis of welding wire scrap contaminated with Sn. Note that Fe content must be compared with ETP copper reference sample. Real Fe content is thus somewhat.

Element							**Average Composition**
Cu (%)	99.989	99.988	99.992	99.990	99.989	99.990	**99.990**
Ag	13.3	14.9	11.6	12.9	14.1	10.3	**12.8**
As	0.30	0.30	0.05	0.25	0.35	0.05	**0.22**
Bi	0.20	0.20	0.20	0.20	0.20	0.2	**0.20**
Fe	17.2	16.3	16.69	16.1	15.3	19.5	**16.8**
Pb	0.32	0.34	0.30	0.30	0.48	0.86	**0.43**
Sb	0.07	0.38	0.07	1.00	0.80	0.61	**0.48**
Se	0	0	0	0.21	0.13	0	**0.06**
Te	0.50	1.47	0.50	1.04	1.68	1.18	**1.06**
Sn	64.9	76.3	48.7	58.5	72.9	43.22	**60.7**
Ni	2.26	2.23	2.50	2.35	2.05	2.26	**2.28**
S	3.39	3.46	2.03	2.42	4.13	3.09	**3.09**
Zn	0	0.01	0	0	0.11	0.49	**0.10**
Al	0.48	0.11	0	0	0.07	2.28	**0.49**
P	0.12	0.28	0.13	0.29	0.40	0.35	**0.26**
Si	4.43	0.89	0.36	0	0.89	15.9	**3.74**
Mn	0	0	0	0.01	0.02	0.03	**0.01**
Cd	0	0	0	0	0	0	**0**
Cr	0.05	0.05	0.04	0.06	0.07	0.30	**0.01**
Be	0.06	0.06	0.07	0.07	0.07	0.07	**0.07**
Mg	0.09	0	0	0	0.03	0.79	**0.15**
Co	0.02	0.03	0.08	0.14	0.09	0.13	**0.08**
Zr	0.12	0.10	0.05	0.12	0.14	0.29	**0.14**
Au	0.08	0.18	0.12	0.23	0.27	0.24	**0.19**

LUNDS
UNIVERSITET